Slow cooling and crystallization of the roots of the Neoproterozoic Araçuaí hot orogen (SE Brazil): Implications for rheology, strain distribution, and deformation analysis

Alain Vauchez, Maria Helena B.M. Hollanda, Patrick Monie, Mathieu Mondou, Marcos Egydio-Silva

Slow cooling and crystallization of the roots of the Neoproterozoic Araçuaí hot orogen (SE Brazil): implications for rheology, strain distribution, and deformation analysis

Alain Vauchez[1], Maria Helena B.M. Hollanda[2], Patrick Monié[1], Mathieu Mondou[1, 2], Marcos Egydio-Silva[2]

(1) Géosciences Montpellier, Université de Montpellier & CNRS, Place E. Bataillon, 34095 Montpellier Cedex 05, France
(2) Instituto de Geociências, Universidade de São Paulo, Rua do Lago, 562, 05508-080 São Paulo, Brazil

Abstract:

The Araçuaí-Ribeira belt formed during the amalgamation of Western Gondwana in the late Neoproterozoic. Its evolution included a main tectonometamorphic peak at 600-580 Ma and a minor peak associated with the final collision with the Western Congo at 540-530 Ma. This belt has the characteristics of a hot orogen, including a high thermal gradient (>30 °C/km), pervasive partial melting of the middle crust, emplacement of large volumes of magmas resulting from partial melting of the lower crust and underlying mantle, and slow cooling after the peak temperature. We report 21 new amphibole, biotite and muscovite $^{40}Ar/^{39}Ar$ ages that complement previously published data. These data suggest slow cooling (3-5 °C/Myr) over several tens of million years after the peak temperature (~800 °C at ~600 Ma) followed by faster cooling (>10 °C/Myr) after the final amalgamation of Western Gondwana. We estimate that ~30 Myr was required to heat the middle crust to the peak temperature and that anatectic and plutonic bodies remained in the magmatic state for ≥ 40 Myr. This protracted thermal evolution likely had major effects on the rheology of the middle crust and on the tectonic evolution of this orogen. For example, the correlation of U-Pb zircon crystallization ages and $^{40}Ar/^{39}Ar$ biotite cooling ages in the anatectic core of the orogen denotes a diachronic thermal evolution likely related to 3D deformation involving successive upwelling of anatectic components within a thrust unit crosscutting the pre-existing fabric ("channel flow-like"). This study also highlights that classical structural analysis techniques relying on changes in pressure or temperature conditions to identify the succession of deformation phases are not efficient at deciphering the tectonic evolution of hot, slowly cooling orogenic belts, where the temperature varies slowly over tens of million years, allowing diachronic episodes of deformation to occur under nearly similar pressure and temperature conditions.

Keywords: Hot orogen, $^{40}Ar/^{39}Ar$ ages, slow cooling, crust rheology, gravity-induced 3D deformation.

1) The Neoproterozoic Araçuaí belt reached a temperature of ≥800 °C at a depth of ~25 km by ~600 Ma
2) The postorogenic peak cooling rate of the Araçuaí middle crust was ~3-4 °C/Myr
3) The middle crust remained partially molten for 40-45 Myr
4) Slow cooling from high temperatures results in low strength, favoring 3D deformation
5) Nearly stable HT conditions over long periods of time may prevent the identification of successive tectonic phases.

Introduction:

Many orogens are characterized by abnormally high geothermal gradients (≥ 30 °C/km) down to the middle/lower crust (e.g., Peucat et al., 1999; Möller et al., 2000; Collins, 2002; Morisset et al., 2009; Högdahl et al., 2012; Turlin et al., 2018). A common characteristic of these "large-hot" orogens (Beaumont et al., 2010) is to have cooled very slowly; estimated cooling rates are usually << 10 °C/Myr (Möller et al., 2000; Morisset et al., 2009, 2014; Guergouz et al., 2018; Turlin et al., 2018). Thus, after the temperature increased to the metamorphic peak, it remained high for millions of years. The effects of this peculiar thermal evolution on the mechanical behavior of the lithosphere and on the petrologic and geochemical systems are still not fully evaluated (Jamieson et al., 2011). Such an evolution contrasts with those of "small-cold" and "alpine-type" orogens (Beaumont et al., 2010), in which the temperature variations during and following the orogeny are much faster. The cooling rates are typically high (several tens of °C/Myr) and sometimes even higher, particularly when rapid exhumation follows orogenesis (e.g., Zeck et al., 1992; Janots et al., 2009). Rapid temperature variations result in marked changes in the rheology of rocks over short periods of time, and successive stages of the orogenic evolution are usually recorded as superimposed deformations occurring under different pressure and temperature conditions. In contrast, in a hot orogen, the temperature decreases very slowly; diachronous deformation episodes may occur under similar temperature conditions and result in similar rock microstructures and mineralogical assemblages. Consequently, it can be difficult to recognize contemporaneous deformations with contrasting kinematics from deformation events separated, for instance, by 10-15 Myr.

The processes that result in the formation of "hot orogens" are still poorly understood. Radiogenic heating of a highly thickened continental crust is regarded as the most efficient process (England and Thompson, 1986; Huerta et al., 1998; Vanderhaeghe et al., 2003; Clark et al., 2011; Clark et al., 2015). However, mechanical heating due to shearing or intrusion of multiple batches of mantle-derived magmas may also contribute to generating abnormally high temperatures (HT) in the middle to lower crust (Michaut and Jaupart, 2007; Nabelek et al., 2010). At larger scales, it has been suggested that slab retreat might trigger upwelling of the asthenospheric mantle, which may contribute to heating of the overlying plate (e.g., Vanderhaeghe and Duchêne, 2010).

Three interacting processes combine to decrease the cooling rates in a hot orogen:

- High temperatures in the middle crust decrease its thermal conductivity and hence its capacity to transfer heat upward. Thus, a "heat reservoir" may form in the middle/lower crust, allowing for maintenance of an abnormal thermal gradient over long periods of time (Michaut and Jaupart, 2007; Whittington et al., 2009; Nabelek et al., 2010).

- High temperatures in the middle to lower crust may trigger widespread partial melting and the generation of large volumes of magma emplaced in the middle crust. During solidification, these magmas release latent heat of crystallization that compensates, at least partially, for conductive cooling (Michaut and Jaupart, 2011).

- The viscosity of a hot and partially molten middle crust is too low to sustain high topography. When the weight of the orogenic topography exceeds the strength of the hot middle to lower crust, it triggers gravity-driven flow that reduces the topography and forms plateaus (e.g., Jamieson et al., 2011 and references therein). This process partly compensates for orogenic thickening of the crust through frontal or/and lateral extrusion; limits erosion rates, and consequently hinders tectonic exhumation and associated cooling.

In Southeast Brazil, the Araçuaí belt (Figure 1) displays evidence of high-temperature contractional deformation distributed almost homogeneously across its internal domain, which is the focus of this study (e.g., Vauchez et al., 2007). The belt is a ~200-km-wide and more than 500-km-long orogenic domain in which pressure-temperature (PT) estimates consistently indicate synkinematic conditions between ~750 °C/500-600 MPa and ≥800 °C/600-700 MPa (Cavalcante et al., 2014; Moraes et al., 2015; Richter et al., 2016), supporting a temperature gradient of 30-35 °C/km to a depth of at least 25 km. Cavalcante et al. (2018) also demonstrated that anatexis was active in the core of the belt for, at least, ~30 Myr. However, the cooling rates are poorly constrained; only two amphibole and three biotite $^{40}Ar/^{39}Ar$ ages from four samples, suggesting low cooling rates, have been published (Petitgirard et al., 2009). Here, we report 21 new $^{40}Ar/^{39}Ar$ ages in amphibole, muscovite and biotite from 16 samples representative of the different tectonic units of the Araçuaí "hot orogen". These new data, combined with previously published U-Pb zircon ages, thermobarometric data, and structural data from field measurements and anisotropy of magnetic susceptibility (AMS) mapping (Vauchez et al., 2007; Petitgirard et al., 2009; Mondou et al., 2012; Cavalcante et al., 2013, 2014, 2018) constrain a protracted tectonothermal evolution for this orogenic belt and confirm that the temperatures in the middle crust remained high over tens of Myr. Based on these results, we discuss the large-scale implications of slow cooling on the evolution of the strain distribution through space and time in this orogenic segment and the difficulties in applying classical tectonic analysis to hot orogens.

Structure of the Araçuaí belt and previous thermochronological data

The Araçuaí belt (Figure 1) is a segment of a large orogenic system that formed between the São Francisco and Congo cratons during the amalgamation of the South America and Africa protocontinents to form Western Gondwana (Hasui et al., 1975; Almeida, 1977; Trompette et al., 1992; Pedrosa-Soares et al., 2007). The bulk orogenic system comprises the Araçuaí-Ribeira and Cabo Frio-West Congo belts (Egydio-Silva et al., 2018). The convergence lasted for at least one hundred million years, and diachronous orogenic climaxes have been substantiated for the Araçuaí-Ribeira orogen (600-570 Ma; e.g., Nalini et al., 2000b; Mondou et al., 2012; Gonçalves et al., 2014; Cavalcante et al., 2018) and for the West Congo belt (540-530 Ma; e.g., Monié et al. 2012). The latter event involved thrusting of the "Cabo Frio Tectonic Domain" onto the eastern Ribeira belt in the Rio de Janeiro state (Schmitt et al., 2004).

On the South American side, the Araçuaí-Ribeira belt forms the eastern to southeastern boundary of the São Francisco craton (Vauchez et al., 1994; Egydio-Silva et al., 2018; Figure 1). The Ribeira belt

forms the southern segment of the orogen. It is characterized by a transpressional tectonic regime that combined orogen-parallel transcurrent motion with orogen-normal thrusting (Vauchez et al., 1994; Egydio-Silva et al., 2002). Seismic anisotropy measurements (Heintz et al., 2003; Assumpção et al., 2006) suggest that orogen-parallel shearing involved the entire lithosphere (Vauchez et al., 2012). To the north, the connection with the Araçuaí belt is characterized by a curvature of the orogenic fabric from NE-SW to N-S (Figure 1) and a progressive transition in the strain regime to dominant westward thrusting of allochthonous units onto the São Francisco craton in the Araçuaí belt (Vauchez et al., 1994; Oliveira et al., 2000; Egydio-Silva et al., 2005, 2018). These longitudinal variations of the orogenic fabric and kinematics are likely related to the southern end of the São Francisco craton (Vauchez et al. 1994). The northern termination of the Araçuaí belt is characterized by dominant northward thrusting of the orogenic units onto the Salvador craton (e.g., Uhlein et al., 1998).

The central Araçuaí belt (Figure 2), where all of the samples used in this study were collected (the locations of selected samples are given in Supplementary Material #1), is composed of four allochthonous domains docked against the São Francisco craton (Brueckner et al., 2000). From west to east, these domains are (Oliveira et al., 2000; Vauchez et al., 2007):

(i) The *para-autochthonous metasedimentary cover* of the craton. Several U-Pb and $^{207}Pb/^{206}Pb$ ages older than 2 Ga obtained in orthogneisses from this domain (e.g., Noce et al., 2000; Silva et al., 2002) and Archean (>2.6 Ga) or Transamazonian (2.1-2.3 Ga) T_{DM} model ages (Brueckner et al., 2000) indicate that the rocks from this unit belong to the craton or to its extended margin. Approaching the contact with the allochthonous units, these rocks display a tectonic fabric parallel to the mylonitic fabric of the westernmost allochthonous unit; the foliation dips gently eastward, and the lineation dominantly plunges to the east (Figure 2; Vauchez et al., 2007). The metapelites contain acicular sillimanite that marks the lineation, garnet, and K-feldspar, and interlayered coarse-grained quartzites contain crystals of sillimanite that are commonly within overgrown quartz grains. Shear indicators, although uncommon, consistently indicate a top-to-the-west sense of shear. This suggests that the eastern part of this unit was strongly deformed under high-temperature conditions during the Neoproterozoic orogeny.

(ii) The *Western Mylonitic Unit (WMU,* Figure 2*)* is the first allochthonous unit that was thrust westward onto the para-autochthonous cover of the craton (Oliveira et al., 2000). This unit comprises mylonites derived from metasediments, which display a foliation that dips gently eastward and bears a down-dip lineation formed under high-temperature and low-pressure (HT-LP) conditions (Petitgirard et al., 2009). The similarity of the lithology and deformation conditions with those of the para-autochthonous cover hinders a precise definition of the basal contact of the WMU. The main differences between the two units are the presence in the WMU of numerous top-to-the-west shear criteria (Figure 3a-d), the absence of quartzites, the alternation of metapelites with amphibolites, and the presence of large volumes (up to 40% locally) of anatectic leucogranites in decimeters-wide veins parallel to the mylonitic foliation (Figure 3b-d). There is no evidence of strain localization at the base of the unit; strain

is rather homogeneously distributed across the WMU. Indeed, the microstructure of the HT mylonites is similar across the entire unit, varying only as a function of the mineralogy.

Petitgirard et al. (2009) estimated the metamorphic conditions for the WMU mylonites based on garnet-biotite exchange thermobarometers; core-core analyses (or biotite included in garnet) consistently yield temperatures of 760-780 °C (±30 °C), and rim-rim analyses temperatures of 730-760 °C (±30 °C) and pressures in the range of 500-600 MPa (±150-200 MPa). A few zircon ages have been published for this unit. Noce et al. (2000) dated two magmatic bodies that intruded into this unit, which yielded ages of 595 ± 3 Ma (Brasilândia pluton) and 574 ± 2 Ma (Guarataia pluton) that were later confirmed by Tedeschi et al. (2016). Petitgirard et al. (2009) dated two synkinematic leucocratic granites intercalated in the mylonites; one yielded a U-Pb age of 577 ± 9 Ma in zircon and 572 ± 3 Ma in monazite, and the other yielded a U-Pb age of 578 ± 3 Ma in zircon (Figure 4; Table 1). These authors reported $^{40}Ar/^{39}Ar$ ages of ca. 501 and ca. 495 Ma for amphiboles and ca. 474 and ca. 468 Ma for biotite from the WMU rocks and from the "Ibituruna" syenite that intruded at the top of the WMU, respectively. These preliminary data are integrated in our database (Table 1, Figure 7) and further commented on (see Supplementary Material #2 for amphibole AR-414 from the Ibituruna syenite).

(iii) The *Central Plutonic Unit* (CPU; Figure 2) comprises large volumes of synkinematic garnet-bearing granodiorites and tonalites that intruded into metasediments (e.g., Mondou et al., 2012; Narduzzi et al., 2017). These plutonic bodies (regionally termed the "São Vitor" and "Galileia" batholiths) display a consistent magmatic fabric (Figure 5) that transitions eastwards from a gently eastward-dipping foliation with a dominantly EW-trending lineation to a steeply dipping to subvertical foliation with a lineation that frequently varies from ~E-W subvertical to ~Ñ-S subhorizontal over intervals of a few tens of meters. In the easternmost part of the CPU, Mondou et al. (2012) substantiated the presence of a corridor in which the magmatic foliation is subhorizontal and bears a strong orogen-parallel, NS-trending magmatic lineation. In several places, the granodiorites and tonalites contain elongated dioritic to gabbroic lenses, implying a contribution of mantle-derived magmas in the formation of the batholiths (Vauchez et al., 2007; Gonçalves et al., 2014; Narduzzi et al., 2017; Figure 5c).

The metamorphic conditions in the metasedimentary rocks of the CPU into which the batholiths intruded are still poorly constrained due to poor outcrop conditions. However, the degree of metamorphism tends to decrease eastwards, as supported by the occurrence of staurolite and, locally, of muscovite in garnet-sillimanite-bearing metapelites of the easternmost part of the CPU. These minerals, indicative of temperatures ≤650 °C (Nalini et al., 2015), are only present in the easternmost CPU.

Several ages have been published for synkinematic granitoids in the CPU emplaced close to the contact with the WMU (regionally termed "Derribadinha"; Table 1; Figure 4). Zircons from two tonalite sills yielded ages of 581 ± 4 Ma and 583 ± 4 Ma (Mondou et al., 2012), which are similar to the ages obtained for leucocratic veins interlayered with mylonitic metasediments (587 ± 5 and 579 ± 8 Ma;

Mondou et al., 2012). An age of 597 ± 4 Ma was obtained for a tonalite sampled ~80 km south of the previous locations and was also ascribed to the Derribadinha domain (Gonçalves et al., 2014).

The São Vitor and Galileia batholiths were emplaced roughly coeval with the Derribadinha granitoids, considering the analytical uncertainties associated with their ages. The São Vitor tonalite was dated at 576 ± 5 and 569 ± 9 Ma (Noce et al., 2000) and at 585 ± 7 and 582 ± 6 Ma (Mondou et al., 2012). The Galileia tonalite/granodiorite was dated at 594 ± 6 Ma (Nalini et al., 2000b). Mondou et al. (2012) dated samples from several domains of this batholith with different fabrics. The U-Pb zircon ages from these domains with different kinematics are fairly consistent between 579 and 583 Ma. Gonçalves et al. (2014) obtained an age of 581±3 Ma for the same tonalitic body as sample AR-787 (582 ± 6; Mondou et al., 2012; table 1).

Finally, two peraluminous granites (the muscovite-biotite-bearing Palmital and the cordierite-garnet-biotite-bearing Wolf leucogranites; Figures 2, 4) were dated at ca. 582 and 585 Ma (Noce et al., 2000). These two granites (Figures 2, 4) are therefore interpreted as resulting from melting of aluminous metapelites contemporaneous with the melting of the lower crust and underlying mantle that formed the tonalitic/granodioritic magmas.

*(iv) Intermediate, discontinuous kinzigitic unit (*Figures 2 and 6). The steeply dipping, medium temperature, staurolite-bearing metasediments that crop out in the easternmost part of the CPU are separated from the gently dipping Eastern Anatectic Unit (EAU; see below) by a laterally discontinuous unit of partially molten kinzigites with a steeply dipping foliation (Oliveira et al., 2000; Mondou et al., 2012). In contrast to the metasediments of the easternmost CPU, these kinzigites contain biotite, garnet, cordierite, and sillimanite but no staurolite or muscovite. The tectonic contact between these kinzigites and the CPU is therefore characterized by a metamorphic jump despite the similar subvertical fabrics in the two units. This suggests that the intermediate kinzigitic unit, which initially equilibrated at deeper levels, was thrust onto the CPU and that the tectonic contact and associated fabric were subsequently rotated to vertical.

(v) The *Eastern Anatectic Unit* (EAU, also known as the "Carlos Chagas leucogranite"; Figures 2 and 6) is more than 300 km long and 50 to 100 km wide. It comprises peraluminous metatexites, diatexites, and leucogranites containing quartz, K-feldspar, garnet, biotite, ± sillimanite, ± rutile, ± cordierite (e.g., Cavalcante et al., 2013). Some garnet-bearing leucogranites are nearly free of biotite (Figure 6c). Rather than a batholith, the EAU represents the anatectic core of the Araçuaí belt, which was intruded by several late orogenic charnockitic plutons (~520 Ma). This unit is characterized by a widespread, penetrative magmatic fabric marked by a magmatic foliation that dominantly dips gently to moderately in various directions due to open folds that affected an initially low-angle foliation (Cavalcante et al., 2013). Detailed mapping of the magnetic foliations and lineations across the EAU revealed a complex flow field characterized by a western domain in which gently dipping foliations bear lineations that progressively rotate from SW in the south to NW in the north (Figure 2) and by an eastern

domain in which subvertical NS-trending foliations bear contain subhorizontal, orogen-parallel lineations (Cavalcante et al., 2013). The eastern boundary of the anatectic unit is defined by a progressive eastward transition to migmatitic kinzigites (Figure 6d) that contain intercalated layers of orthopyroxene-bearing granulites.

Cavalcante et al. (2014, 2018), using the Ti-in-quartz (TitaniQ) and Zr-in-rutile geothermometers in the anatexites and Fe-Mg exchange geothermobarometers in the neighboring kinzigites, obtained temperatures of 780-800 °C and pressures in the range 650-700 MPa, which were interpreted as the P-T conditions under which crystallization of the anatexites began during cooling. These estimates are in good agreement with those obtained for migmatitic kinzigites by Munhá et al. (2005) using Fe-Mg exchange geothermobarometers and, more recently, by Richter et al. (2016) from phase equilibrium modeling. The presence of cordierite and rutile in the studied rocks, which crystallize at T ≥ 760°C (Le Breton and Thompson, 1988; Harley et al., 2002; Pattison et al., 2003; Harley, 2004), as well as evidence of destabilization of restitic biotites found in several diatexites, all support temperatures > 800°C (Le Breton and Thompson, 1988; Vielzeuf and Holloway, 1988; Pattison et al., 2003). As highlighted by Cavalcante et al. (2014), high temperatures probably allowed for melt fractions greater than 30%, which should drastically reduce the viscosity of the anatectic middle crust (Rosenberg and Handy, 2005; Vanderhaeghe, 2009).

Numerous SHRIMP U-Pb zircon ages are available for the EAU anatexites (Vauchez et al., 2007; Cavalcante et al., 2018), and they substantiate broad variability across the entire domain. Several diatexites and anatectic granites yielded ages in the range of 597-593 Ma, and others (including one metatexite) were dated between 589 and 572 Ma. On average, the ages are older in the northwest and younger in the southeast, but the trend is still not well defined (Figure 5). Richter et al. (2016) reported a similar age range (595-570 Ma) for samples from the easternmost "Nova Venecia" kinzigitic unit of the Araçuaí belt. Together, these U-Pb data argue that anatexis was already underway in the middle crust (~25 km) of the Araçuaí belt by ~600 Ma and that it remained active until at least ca. 570 Ma (Cavalcante et al., 2018).

$^{40}Ar/^{39}Ar$ ages

For this study, we collected ten samples across the CPU, including two synkinematic tonalites from the contact between the CPU and the WMU, five synkinematic granodiorites/tonalites with a well-developed magmatic fabric from the São Vitor and Galiléia batholiths, one synkinematic leucogranite (the Wolf granite), one muscovite-bearing peraluminous granite (the Palmital pluton), and one orthogneiss from the country rock (Figure 7). Six of these samples have U-Pb zircon ages close to 580 Ma (Mondou et al., 2012). $^{40}Ar/^{39}Ar$ ages were obtained for amphibole from four tonalites, muscovite from the Palmital leucogranite, and biotite from all of the samples (see Table 1).

For the EAU, we obtained $^{40}Ar/^{39}Ar$ ages only for biotite because amphibole was not found in the anatexites. We selected six of the twelve samples dated by Cavalcante et al. (2018), which include four

anatectic granites, one diatexite and one metatexite (Figure 4, Table 1). The locations of all of the samples dated in this study as well as the 2 amphibole and 3 biotite ages obtained by Petitgirard et al. (2009; Table 1) are shown in Figure 7. Samples from the CPU were analyzed at Geosciences Montpellier (University of Montpellier, France), and those from the EAU were analyzed at the Geochronological Research Center of the University of São Paulo (Brazil). The $^{40}Ar/^{39}Ar$ diagrams are shown in Figures 9 and 10, and the complete analytical data are available in the Supplementary Material #3 and #4.

The $^{40}Ar/^{39}Ar$ cooling ages of the CPU show a larger dispersion (~550 to 470 Ma) than the U-Pb ages from zircon (Figure 7). This dispersion reflects both the difference in closure temperatures between amphibole and micas and the variability from sample to sample. The amphiboles from all of the tonalite/granodiorite samples provide nearly undisturbed age spectra with plateau ages ranging from 549.2 ± 5.6 Ma to 500.4 ± 4.5 Ma (Figure 8). The single analyzed muscovite, which was from the Palmital leucogranite, yields a plateau age of 487.6 ± 4.5 Ma for more than 90% of the released ^{39}Ar (Figure 8), while the biotite age overlaps at 484.1 ± 4.7 Ma with the one of the orthogneiss (484.3 ± 5.2 Ma), The Wolf leucogranite yields an $^{40}Ar/^{39}Ar$ biotite age of 491.9 ± 5.8 Ma, and the biotites from the São Vitor and Galileia batholiths yield $^{40}Ar/^{39}Ar$ ages between 489.5 ± 5.4 Ma and 474.5 ± 4.4 Ma. Two samples of tonalite collected near the contact between the WMU and the CPU yield older cooling ages for amphibole (549.2 ± 5.6 and 541.6 ± 7.7 Ma) and biotite (532.2 ± 5.4 and 507.5 ± 5.3 Ma). Although reliable from the analytical point of view, the geological significance of these older ages remains unclear because neighboring samples, collected on both sides of this contact, yield younger amphibole and biotite cooling ages (Figure 7).

In the EAU, the $^{40}Ar/^{39}Ar$ ages in biotite span from 485.8 ± 4.4 Ma to 458.5 ± 4.2 Ma with the oldest age obtained for the northernmost sample and the youngest for the southernmost sample (Figure 9; Supplementary Material #4). This distribution correlates quite well with the variation in U-Pb zircon ages across this domain (Cavalcante et al., 2018).

Discussion

4.1. The heating episode

Considering the current crustal thickness of ~40 km (Assumpção et al., 2013) and the paleopressures of 0.6-0.7 GPa recorded by rocks currently exposed in the central Araçuaí orogen (Petitgirard et al., 2009; Cavalcante et al., 2014; Richter et al., 2016), the inferred orogenic crustal thickness was likely greater than 60 km. Temperatures of 740 °C to ≥ 800 °C were recorded at depths of 20-25 km (Petitgirard et al., 2009; Cavalcante et al., 2014; Richter et al., 2016), suggesting an average thermal gradient higher than 30 °C/km within the upper and middle crust. The thermal gradient was likely significantly lower in the lower crust and underlying mantle (Whittington et al., 2009). Throughout the orogen, the magmatic bodies are either embedded in metapelitic rocks (WMU and CPU) or formed by anatexis of metapelitic rocks (EAU). This implies that the orogenic middle crust of the Araçuaí belt, to a depth of at least 25 km, was mostly composed of metapelites with some intercalated layers of

amphibolites and quartzites. Although the content of heat-producing elements of these metapelites is not known, we hypothesize that it would have been high enough to contribute significantly to heating (Clark et al., 2011, 2015). As a result, the middle crust would have undergone prograde metamorphic dehydration reactions favoring extensive water-present partial melting in domains where water migrated (Weinberg and Hasalová, 2015).

The presence of lenses of diorite/gabbros within the granodioritic/tonalitic magmas (Figure 5c) indicates that partial melting also affected the underlying mantle (Mondou et al., 2012; Gonçalves et al., 2014). The initiation of heating in the lithospheric mantle might have resulted from preorogenic enrichment of the subcrustal mantle in heat-producing elements due to metasomatic reactions (Neves et al., 2008) during the Neoproterozoic episode of rifting of the lithosphere along the eastern border of the São Francisco craton that preceded the orogeny (Cunningham et al., 1996; Uhlein et al., 2007).

Available U-Pb zircon ages are remarkably consistent across the various geological units that shape the central part of the Araçuaí orogen. Similar ages have been reported in the northern (Siga Jr et al., 1987) and southern portions of the belt, including its connection with the Ribeira transpressional belt (Silva et al., 2005; Bento dos Santos et al., 2010). Ages obtained in the EAU (Cavalcante et al., 2018) and in the "Nova Venecia" easternmost kinzigitic domain (Richter et al., 2016; Melo et al., 2017) indicate that by ca. 600 Ma, the middle/lower crust of the Araçuaí orogen had reached temperatures higher than 800 °C and was already partially molten, producing garnet-rich aluminous magmas. Following this metamorphic peak, huge volumes of granodioritic/tonalitic magmas were emplaced in the CPU between 590 and 570 Ma (mostly between 585-575 Ma); i.e., coeval with pervasive partial melting of the middle crust that formed the anatectic core of the belt. The magmatic fabric of these rocks, although variable through the entire CPU, is always parallel to the solid-state fabric of their country rocks and of the neighboring units (mylonites of the WMU and kinzigites of the intermediate unit between the CPU and EAU). Thus, structural and geochronological data consistently indicate that the profuse magmatism that characterizes the CPU was emplaced during the main deformation that built the Araçuaí orogen and the synchronous anatexis of the middle/lower crust (Vauchez et al., 2007; Mondou et al., 2012; Cavalcante et al., 2018). Therefore, the tonalitic/granodioritic magmatism of the CPU cannot represent a preorogenic magmatic arc, as suggested by Pedrosa-Soares and Wiedemann-Leonardos (2000). These magmas should have formed during the orogeny, likely through mixing of magmas resulting from partial melting of the lower crust and subcrustal mantle, as evidenced by the presence of numerous cm- to m-sized lenses of dioritic and gabbroic magmas. The Sr and Nd isotope compositions of such rocks suggest that their parental magmas were derived mainly from melting of older crust (Nalini et al., 2000), even though the proportions of crustal and mantellic components are not known (Gonçalves et al., 2014). Thus, the process responsible for this synkinematic magmatism remains unknown.

The U-Pb zircon ages of the anatectic rocks from the EAU suggest that contractional tectonics and crustal thickening initiated significantly earlier than 600 Ma. A rough estimate of the initiation of this episode may be obtained based on data from the EAU considering heating rates in the range of 5-

20 °C/Myr (Harris et al., 2000 and references therein) or 8-15 °C/Myr, as recently deduced from allanite and monazite dating in the central Alps by Janots et al. (2009). Assuming an initial temperature of approximately 400 °C at depths of 20-25 km (McKenzie et al., 2005), heating up to 800 °C would have required between 27 and 50 Myr. For a higher initial temperature (i.e., 500 °C at 20-25 km), such as due to preorogenic rifting, 20-38 Ma would have been needed. This would imply that the deformation producing thickening and prograde metamorphism in the Araçuaí belt started significantly before 620 Myr ago. Such a delay between the initiation of the orogeny and the occurrence of widespread partial melting is consistent with estimates from models for southern India developed by Clark et al. (2015). It is also consistent with the time intervals (20-60 Myr) between the initiation of collision and melting of the middle/lower crust under peak metamorphism conditions estimated for southern Tibet and the High Himalayas and for the Canadian Cordillera (e.g., Vanderhaeghe and Teyssier, 2001b and references therein; Zhang et al., 2004; Guo and Wilson, 2012).

The younger ages obtained for the late- and post-collisional granitic bodies (Silva et al., 2002, 2005; Mondou et al., 2012) highlight that magmatic pulses occurred over more than 100 Myr until at least 500 Ma. Among the late magmatic bodies, the origins of the "Ibituruna" syenite in the CPU (529.9 ± 1.3 Ma; Petitgirard et al., 2009) and the "Padre Paraíso" charnockitic suite that crosscuts the belt (ca. 520 Ma; Noce et al., 2000; Mondou et al., 2012) are still poorly understood. Nevertheless, their compositions imply that relatively high-temperature conditions subsisted in the lower crust and underlying mantle up to these late stages of the evolution of the Araçuaí belt. Interestingly, these late magmatic events are coeval with the main tectonometamorphic event in the West Congo belt in Angola (Monié et al., 2012) and in the "Cabo Frio Tectonic Domain" (Schmitt et al., 2004). Therefore, they might record limited reactivation of the Araçuaí belt in response to the formation of the "Congo-Cabo Frio" belt during the final collision between the African and South American protocontinents at 540-530 Ma.

4.2. Cooling rates

To estimate the cooling rates in the Araçuaí belt, we consider only the U-Pb and $^{40}Ar/^{39}Ar$ ages obtained by our group (Table 1; Vauchez et al., 2007: Petitgirard et al., 2009; Mondou et al., 2012; Cavalcante et al., 2018; this work), for which the locations of samples, the definitions of the rock types and, in the case of the magmatic rocks, the synkinematic or postkinematic emplacement and absence of solid-state reworking are well known. This choice does not modify the interpretations referred to here because there is good agreement between our data and those from previous studies.

As a priori information, we use the equilibrium temperatures estimated for the metamorphic country rocks (~750 °C; Petitgirard et al., 2009) and the U-Pb zircon ages of synkinematic magmas in the WMU (577-578 Ma; Petitgirard et al., 2009) to define the minimum starting temperature of the cooling path. For the EAU, we consider two age-temperature intervals: (1) U-Pb ages of 597-593 Ma and temperatures of 800-790 °C (Cavalcante et al., 2014, 2018) for the oldest anatexites and (2) U-Pb ages of 578-570 Ma and temperatures of 740-720 °C (Cavalcante et al., 2018) for the youngest ones. For the samples with intermediate U-Pb ages (589-583 Ma), we estimated the temperature assuming progressive

cooling between groups (1) and (2). For (1), the temperatures are not necessarily representative of the peak metamorphic conditions but rather of the initiation of crystallization and thus cooling of the magmas. However, the temperatures for the WMU provide a reliable estimate of the starting temperatures of the cooling path in the EAU, while the temperatures calculated from the youngest anatexites represent the minimum values at this time.

Figure 10 summarizes all of the ages obtained by our group for the Araçuaí belt. The U-Pb zircon ages from the synkinematic leucogranites in the WMU mylonites, granodiorites/tonalites from the CPU, and anatexites from the EAU range from ~600 Ma to ~570 Ma with a clear concentration between 585 and 575 Ma (19 of 29 ages), indicating that the metamorphic peak, partial melting, and tonalitic/granodioritic magmatism occurred during this time period. To estimate a mean cooling rate, we use the median value of 584 Ma (σ = 7) calculated based on 27 zircon ages. The ages of the late Ibituruna syenite (AR-414) and the orthogneiss AR-722 (2103 ± 11 Ma; Mondou et al., 2012) were excluded. In contrast, the $^{40}Ar/^{39}Ar$ age of this Paleoproterozoic orthogneiss was also considered because it is similar to those provided by the magmatic biotites.

$^{40}Ar/^{39}Ar$ ages from amphibole and micas record cooling through their respective closure temperatures. A first estimate of the cooling rate was obtained considering closure temperatures of 550 ± 30 °C for amphibole (Dahl, 1996), 400 ± 20 °C for muscovite (Harrison et al., 2009), and 325 ± 20 °C for biotite (Harrison et al., 1985). However, for very low cooling rates, isotopic re-equilibration may continue at temperatures lower than the experimental closure temperature (Dodson, 1973). Thus, we recalculated the closure temperatures for amphibole, muscovite and biotite taking into account a range of cooling rates (5 °C/Myr for amphibole and 15 °C/Myr for biotite and muscovite) and the grain sizes of the dated minerals measured in thin sections (Brandon et al., 1998; McDougall and Harrison, 1999; Braun et al., 2006; Reiners and Brandon, 2006). Consequently, the closure temperatures are updated to 458 to 531 °C for amphibole, 418 ± 10 °C for a single analyzed muscovite and 283 to 338 °C for biotite (Table 1).

The average cooling rates inferred for the various scenarios are shown in Figure 10:

- The first scenario (curve 1) considers average ages of 584 Ma (U-Pb zircon age), 510 Ma ($^{40}Ar/^{39}Ar$ amphibole) and 487 Ma ($^{40}Ar/^{39}Ar$ biotite), 505 °C as the average closure temperature of amphibole and 317 °C as the average closure temperature of biotite. These data provide cooling rates of 4 °C/Myr with an initial temperature (T_i) of 800 °C between 584 and 510 Ma (3.3 °C/Myr assuming T_i = 750 °C) and of 8.2 °C/Myr between 510 and 487 Ma.
- For the second scenario (curve 2), we excluded the two samples that yielded significantly older $^{40}Ar/^{39}Ar$ amphibole and biotite ages and used average closure temperatures of 503 °C for amphibole and 317 °C for biotite. The obtained cooling rates are 3.5 °C/Myr between 584 and 499 Ma with T_i = 800 °C (2.9 °C/Myr assuming T_i = 750 °C) and 9.8 °C/Myr between 499 and 480 Ma.
- Even considering only the oldest ages obtained for amphibole (average: 546 Ma) and biotite (average: 520 Ma), the cooling rates still remain low (curve 3): 7.8 °C/Myr between 583 and

546 Ma with T_i = 800 °C (6.4 °C/Myr for T_i = 750 °C). The cooling rates below the closure temperature of amphibole range between 16.8 °C/Myr (using the biotite age of 532 Ma from sample AR-590) and 5.9 °C/Myr (using 508 Ma from sample AR-1057). An average cooling rate of 8.3 °C/Myr is calculated using an average biotite age of 520 Ma.

Local cooling rates for the EAU can be estimated using $^{40}Ar/^{39}Ar$ biotite ages of six samples presented herein that are matched by U-Pb zircon ages between 597 and 572 Ma (Table 1; Figures 7, 9). The $^{40}Ar/^{39}Ar$ ages range from 486 to 459 Ma, and the average closure temperatures vary from 306 to 336 °C (Table 1). If we consider the oldest anatectic leucogranites of the EAU (AR-1133; curve 4 on Figure 10), which has a U-Pb zircon age of 597 ± 3 Ma, an $^{40}Ar/^{39}Ar$ biotite age of 486 ± 4, a TitaniQ temperature of ~800 °C as an initial temperature (Cavalcante et al., 2014), and a biotite closure temperature of 306 °C, we obtain an average cooling rate of ~4.5 °C/Myr over a period of time greater than 110 Myr after the crystallization of zircons from the anatectic melt. This cooling rate is nearly the same as that obtained from sample AR-1349, for which an equilibrium temperature of 780-790 °C was estimated using Zr-in-rutile data (Cavalcante et al., 2018); it has a U-Pb zircon age of 583 Ma and an $^{40}Ar/^{39}Ar$ biotite age of 476 Ma (closure temperature: 330 °C), pointing to an average cooling rate of ~4.3 °C/Myr. For the youngest anatectic sample (AR-1370), the U-Pb zircon age of 572 Ma, the $^{40}Ar/^{39}Ar$ biotite age of 469 Ma with a closure temperature of ~ 307 °C, and a minimum temperature of ~720 °C assumed from Ti-in-zircon data (Cavalcante et al., 2018) suggest cooling by ~413 °C over 103 Myr and therefore to an average cooling rate of 4 °C/Myr.

The cooling rates estimated for the EAU lack intermediate constraints between zircons and biotite and therefore consider linear cooling between early crystallization in the melt and the isotopic closure of the K/Ar system in biotite. Considering the difference in cooling rates above and below the closure temperature of amphibole obtained for rocks from the WMU and the CPU, a cooling rate significantly lower than 4 °C/Myr may also be expected for the EAU during the first tens of million years after the peak metamorphism.

In summary, the absolute ages and metamorphic temperature estimates from the three allochthonous units consistently suggest low cooling rates (~3 to 8 °C/Myr; likely 3-5 °C/Myr) during at least the first 40 Myr after the initiation of cooling (based on the oldest $^{40}Ar/^{39}Ar$ ages of amphiboles - Am3 in Figure 10) and likely 70-80 Myr (based on the average $^{40}Ar/^{39}Ar$ age of amphibole - Am1 in Figure 10) or even >100 Myr in the EAU. These data also imply that the cooling was faster (at least 11-15 °C/Myr) after the closure of the K/Ar system in amphibole and possibly even faster (> 20 °C/Myr) approaching the closure temperature of muscovite, although the latter inference requires further investigation since it relies on the muscovite $^{40}Ar/^{39}Ar$ age of only one sample in our database. However, the cooling rates were likely lower immediately after the metamorphic peak, especially due to the release of the latent heat of crystallization during progressive solidification of magmatic rocks, the injection of new batches of magma (Michaut and Jaupart, 2011) and the slow exhumation due to gravity-induced deformation that reduced the topography and thus limited the rate of exhumation during tens of millions of years. After the crystallization of large

volumes of synkinematic magmas, cooling became progressively faster over time. However, although no evidence has been found yet, episodes of reheating cannot be ruled out. For example, Melo et al. (2017) argued that a second episode of partial melting occurred at ~530 Ma in the Carlos Chagas domain (EAU).

These estimates of the cooling rates in the Araçuaí belt are in relatively good agreement with those proposed by Bento dos Santos et al. (2010; 2014) for anatexites, granulites, and charnockites from the northern Ribeira belt. These authors propose a two-step thermal evolution with initial cooling rates of 1-5 °C/Myr for 50-90 Myr followed by faster cooling by 8-30 °C/Myr and possibly up to 100 °C/Myr based on diffusion of Fe^{2+} and Mg between garnet and biotite inclusions. Although the approaches are different, the estimates obtained in these two segments of the Ribeira-Araçuaí orogen (Egydio-Silva et al., 2018) consistently indicate very slow cooling for several tens of million years after the major high-temperature deformation that shaped the Araçuaí and the northern Ribeira belts.

The $^{40}Ar/^{39}Ar$ ages of 498-493 Ma for amphibole and of 487 to 466 Ma for biotite obtained in the West Congo belt in Angola (Monié et al., 2012) are similar to those obtained in the Araçuaí belt, suggesting that although the ages of the orogenic/metamorphic peaks are different in these two belts (Araçuaí: 600-580 Ma; West Congo: ~540-530 Ma), they shared a common cooling history after the final amalgamation of Western Gondwana.

4.3. Effect of protracted high-temperature conditions in the middle crust on its rheology and strain distribution

Under "hot orogen" conditions (i.e., high temperatures and low cooling rates in the middle and lower crust), we may expect specific rheological behaviors. When the temperature gradient reaches peak conditions, the temperature is nearly homogeneous over large volumes both laterally and vertically (e.g., Whittington et al., 2009). Rheological contrasts between different crustal rock types are minimized, and the strain localization efficiency, which is inversely proportional to stress and thus to temperature, becomes much lower. Strain tends to be distributed over large volume of rocks (Vanderhaeghe and Teyssier, 2001a). Consequently, the transitions between orogenic domains should be much smoother than under lower temperature conditions (Vanderhaeghe and Teyssier, 2001b). This is particularly true when the middle to lower crust undergoes widespread partial melting because this process may lead to a decrease in viscosity by several orders of magnitude (e.g., Rosenberg and Handy, 2005; Rosenberg et al., 2007; Cavalcante et al., 2014), even in the presence of a small proportion of melt. For instance, through reinterpretation of experimental data from partially molten systems, Rosenberg and Handy (2005) pointed out that the strength of a rock decreases drastically during the first ~7% of partial melting. They also argued that similarly, the strength of magmas deforming during crystallization remains low until they reach a proportion of solid-phases of ~90% and then increases rapidly up to the solidus. When cooling is slow, as in the case of the Araçuaí orogen, high melt fractions persist for long times, and partially crystallized magmatic bodies or partially molten anatexites may accommodate most of the strain, either gravity-induced or due to far-field forces, during most of the convergence.

The three main allochthonous units of the Araçuaí orogen are characterized by the presence of large volumes of synkinematic magmas intermingled with metasedimentary rocks, including leucogranites interlayered with mylonites in the WMU, granodiorites/tonalites in the CPU, and anatexites in the EAU. Such large volumes of magmas in the middle crust certainly had a major impact on the rheology of the orogenic lithosphere. Using the cooling rates discussed in the previous section, we may roughly estimate the time period between emplacement and solidification of the magmas. For instance, the oldest anatectic granite of the EAU, which was emplaced at ~597 Ma in the middle crust at a minimum temperature of 800 °C, yields a mean cooling rate of 4.5 °C/Myr, suggesting that the solidus temperature (~630 °C) was attained at least 40-45 Myr after its emplacement (i.e., at approximately 550-555 Ma). Time periods in the range of 30-40 Myr are obtained considering the synkinematic leucogranites of the WMU and the tonalite and granodiorites of the CPU emplaced at ~580 Ma in mylonites or metasediments that equilibrated at ~750 °C and cooled at 3-4 °C/Myr. The consistent estimates for the different units of the Araçuaí belt support that the large volumes of magmas emplaced or formed in the three allochthonous units allowed for magmatic flow and hence maintained low strengths in the middle crust for ~40 Myr after the initiation of cooling. Considering the suggestion of Ackerson et al. (2018) that granitic and granodioritic rocks may contain significant volumes of interstitial magma down to temperatures as low as ~500 °C, this time period may still be underestimated. Indeed, in the Grenville Province in North America, cooling rates in the range of 2.3-4.4 °C/Myr and the maintenance of suprasolidus conditions over ≥ 70 Myr have been estimated (Turlin et al., 2018). As deduced from seismic profiles (Nelson et al., 1996), the presence of a partially molten middle crust beneath Tibet due to partial melting that initiated 20-25 Myr ago (Zhang et al., 2004; Guo and Wilson, 2012) illustrates that a long-lived partially molten crust may have been present in orogens of a variety of ages.

The increase in viscosity upon cooling may generate a strength inversion between the magmatic bodies and their country rocks. For instance, Nabelek and Liu (2004) suggested an inversion of shear strength between a mica schist and a dry granite at a temperature of ca. 530 °C that depends weakly on the strain rate. Based on the cooling rates estimated from our data, a strength inversion between the metapelitic country rocks and magmatic bodies might have occurred as late as 60 Myr after emplacement of the magmatic bodies. The magmatic bodies were therefore the most deformable part of the middle crust for several tens of million years. Considering the large volumes of magma present in the middle crust during the main deformation, the magmatic bodies had sufficient continuity to accommodate a large proportion of the strain imposed by both plate tectonics and gravity. Interestingly, although these synkinematic magmas show evidence of pervasive deformation in the magmatic state, they are usually free of evidence of solid-state deformation (Mondou et al., 2012; Cavalcante et al., 2013, 2018). Only few samples display intracrystalline microstructures such as undulose extinction or subgrain boundaries in feldspar that commonly record deformation during the last stages of crystallization (Blumenfeld and Bouchez, 1988). Such observations likely indicate that the main deformation ended significantly before the synkinematic magmas reached the solid-state; i.e., before ~550 Ma.

The viscosity increase during cooling in a hot orogen may also lead to a progressive decrease of the contribution of gravity-driven forces to regional deformation, so the strain regime progressively becomes dependent on far-field forces only. Strengthening of the middle crust might also have allowed more effective transmission of tectonic forces toward the external domains of the orogen during the late stages of the orogenic evolution. However, the Neoproterozoic deformation of the remobilized eastern border of the São Francisco craton is still poorly constrained, and this hypothesis requires further investigation to be confirmed.

4.4. Tectonic evolution of the Araçuaí belt

The low cooling rates estimated in this study and their possible rheological consequences require reconsidering the tectonic evolution of the Araçuaí belt. As stated above, a characteristic of this orogenic segment is that strain occurred under high-temperature conditions in the presence of syntectonic magmas and was nearly evenly distributed across the tectonic units described previously. However, detailed mapping revealed that the tectonic fabric is variable across the belt. In particular, in the CPU and EAU, the foliation and lineation form a complex pattern suggesting 3D deformation (Mondou et al., 2012; Cavalcante et al., 2013). Even if domains with different tectonic fabrics display consistent HT conditions of deformation and similar U-Pb ages of synkinematic magmas, the question of their contemporaneity remains open because this study points that HT conditions were maintained for several tens of millions of years. In partially molten rocks, a new deformation event tends to erase evidence of any previous event. Rapid diffusion, which allows for easy grain boundary migration, may have similar effects in HT metamorphic rocks. Under such conditions, it is difficult to establish a reliable chronology of deformation since classical techniques of structural analysis are less efficient than in faster-cooling orogenic belts.

Despite the homogeneity of the rock types, equilibrium temperatures, and systematic deformation in the magmatic state throughout the entire EAU, the geochronological data denote a diachronous tectonothermal evolution within this unit. There is a clear correlation between the southeastward decrease in zircon ages shown by Cavalcante et al. (2018) and the variation in $^{40}Ar/^{39}Ar$ biotite ages across the EAU. The samples with the oldest U-Pb zircon ages were the first to reach the closure temperature of biotite, while the samples with the youngest U-Pb ages yield the youngest $^{40}Ar/^{39}Ar$ biotite ages (Figure 11). Only the $^{40}Ar/^{39}Ar$ age of the biotite from the anatectic granite AR-535 does not follow this trend, displaying a younger than expected biotite $^{40}Ar/^{39}Ar$ age that might be due to the vicinity of a large body of charnockite emplaced at ~520 Ma. The presence of this hot magmatic body may have reduced the cooling rate in the surrounding rocks during its solidification. There is no evidence of such a correlation between U-Pb and $^{40}Ar/^{39}Ar$ ages in the WMU and CPU, suggesting that the EAU underwent a specific tectonothermal evolution.

The variations in U-Pb and $^{40}Ar/^{39}Ar$ ages suggest that although they were not far from each other, some parts of the EAU started to crystallize and cool significantly before other parts. This might be due to diachronous migration of the granites generated in the anatectic middle crust or to small-scale convection in the anatectic core of the belt (Riel et al., 2016). However, considering the complex strain pattern

mapped across the EAU (Cavalcante et al., 2013), the variation in thermal evolution in this tectonic unit is in good agreement with a 3D tectonic-flow model proposed by Cavalcante et al. (2013, 2018). This "channel flow-like" model differs from the initial "channel flow" model (Beaumont et al., 2001, 2004) because the anatectic unit is overlain by the easternmost kinzigitic "Nova Venecia" unit that was thrust above the EAU. Consequently, the deformation of this unit is more similar to Taylor-Couette flow than to the initial Poiseuille flow model (Beaumont et al., 2001). During westward thrusting of the eastern domain of the belt onto the CPU (Figure 12), due to gravity forces some parts of the anatectic core of the belt were pushed upwards before, or more efficiently than, other parts. The western EAU anatexites, which were in an initially shallower position, crystallized zircon and reached the closure temperature of biotite before the initially deeper eastern EAU. In addition, the regional variation in ages implies that the transcurrent fabric mapped in the eastern EAU (Cavalcante et al., 2013; Figure 2) likely formed after the gently dipping foliations of the western part of the EAU, even if the strain was accommodated by magmatic flow in the anatexites in both cases.

The "channel flow-like" interpretation for the deformation of the EAU is consistent with the large-scale structure of the belt and with the crosscutting relationships of the contacts between the different units (Figure 12), which suggest diachronous deformation under suprasolidus temperatures across the belt. The anatexites of the EAU discordantly cover the other allochthonous units. In the northernmost part of the Araçuaí belt, they directly overlie the para-autochthonous HT metasediments of the São Francisco craton (Figure 12a), while in the central part of the Araçuaí belt, the EAU is thrust over the subvertical contact between the western CPU and the higher-temperature intermediate kinzigitic unit (Figure 12b). This supports earlier thrusting of the deeper intermediate kinzigitic unit over the CPU, subsequent rotation of the contact to vertical, and finally thrusting of the anatexites of the EAU onto the steeply dipping structures of the central and intermediate units. No evidence of significant solid-state deformation associated with thrusting of the EAU over the other units has been observed in the various EAU anatexites, which are solely characterized by a strong magmatic fabric. This scenario suggests that these events, although diachronous, occurred before complete solidification of the magmatic bodies in the different units and that the deformation was always concentrated in the partially molten (or crystallized) rocks.

Conclusions

Twenty-one new $^{40}Ar/^{39}Ar$ ages of amphibole, muscovite and biotite from 16 samples collected in the central (CPU) and eastern (EAU) units of the Araçuaí belt, together with $^{40}Ar/^{39}Ar$ and U-Pb ages and P-T data previously published by our group (Vauchez et al., 2007; Petitgirard et al., 2009; Mondou et al., 2012; Cavalcante et al., 2013, 2014, 2018), provide constraints on the thermal history of the middle crust in the central part of the Araçuaí hot orogen. The U-Pb zircon ages suggest that by ~600 Ma, the middle to lower crust, which had been heated to temperatures of ~800 °C, was already partially molten and that production of anatectic magmas persisted until at least ~570 Ma (Cavalcante et al., 2018). The granodioritic/tonalitic magmatism of the CPU, as well as the synkinematic leucogranites within the

mylonitic metasediments of the WMU, were emplaced during this period (Nalini et al., 2000a, b; Noce et al., 2000; Petitgirard et al., 2009; Mondou et al., 2012; Gonçalves et al., 2014).

Altogether, these data denote a protracted orogenic evolution marked by:

- Initiation of crustal thickening and heating of the middle crust at ~630-620 Ma,
- Heating of the middle crust to ≥800 °C and initiation of pervasive partial melting at ~600 Ma,
- Partial melting remaining active until at least ~570 Ma; it affected the middle and lower crust as well as the mantle, as deduced from the mixing of magmas that formed the tonalitic/granodioritic plutonic bodies,
- Slow cooling (3-5 °C/Ma) of the middle crust, which reached temperatures of ~500 °C at 510-500 Ma and ~300 °C at ~480 Ma. These slow cooling are incompatible with fast exhumation of the roots of the orogen.
- The magmatic rocks maintained high melt fractions for several tens of Myr (> 40 Myr), during which they accommodated most of the imposed deformation by magmatic flow. A rough estimate suggests that they reached the solidus temperature (~630 °C) at ~545-555 Ma.
- The anatexites of the EAU underwent a diachronic evolution; those from the northwestern part crystallized and cooled earlier than those from the southeastern part. However, the estimated cooling rates across the EAU are similar. This evolution is consistent with a diachronic upward migration across the anatectic unit as it was thrust westward onto the central domain. Diachronic upwelling of anatectic rocks due to gravity forcing, such as in the "channel flow" model, is compatible with the low viscosity and the resulting 3D deformation of anatexites documented by Cavalcante et al. (2013, 2014, 2018).

Such a protracted thermal evolution had major effects on the rheology of the orogenic crust, on strain partitioning across the belt, and thus on the tectonic evolution of the Araçuaí belt. During progressive heating of the orogenic crust (prograde metamorphism), deformation was already active, and crustal thickening was accommodated in the metasedimentary sequence, but the microstructures recording these early stages of deformation are difficult to differentiate from those formed at the peak of metamorphism in the presence of melt and during subsequent deformation under nearly stable temperature conditions. The initiation of partial melting at ~600 Ma and syntectonic injection of large volumes of granodioritic/tonalitic magmas between 590 and 570 Ma greatly decreased the viscosity of the middle crust, allowing gravity-induced deformation to combine with far-field compressive forces to produce a 3D deformation regime (Cavalcante et al., 2013). This may explain toward the northward termination of the Araçuaí belt, the tectonic flow recorded in the middle crust rotates from dominantly westward onto the São Francisco craton to northward onto the Salvador cratonic block (e.g., Uhlein et al., 1998).

Similar $^{40}Ar/^{39}Ar$ cooling ages have been obtained for biotite in both the Araçuaí belt in Eastern Brazil and the West Congo belt in Angola (Monié et al., 2012) despite the large differences in the ages of the orogenic climax and in the tectonic evolution. This suggests that the late thermal evolution in the Araçuaí - Ribeira orogen was shared by the West Congo - Cabo Frio belt during the final stages of

continental amalgamation. This might explain the late emplacement of several atypical magmatic bodies (e.g., syenites, charnockites) in the Araçuaí belt.

Acknowledgements: We are indebted to Andréa Tommasi for her critical reviews and comments on successive versions of this manuscript. We warmly acknowledge Olivier Vanderhaegue and an anonymous reviewer for their detailed reviews and their suggestions to improve our manuscript. We also thank Carolina Cavalcante and Sylvain Petitgirard for their important contributions to the study of the eastern anatectic and western mylonitic units, respectively. This study benefited from funding by CAPES-COFECUB project Te 588/07 and by FAPESP through grant 2005/56372-7. M.H.B.M. Hollanda thanks CNPq for her research grant.

Figure captions

Figure 1: Schematic map of the Neoproterozoic tectonic belts in eastern Brazil. The Brasilia belt is docked against the western and southwestern boundaries of the São Francisco (SF) craton. The Ribeira/Araçuaí belt formed along the eastern and southeastern boundaries of the craton. The transition between the Araçuaí and Ribeira orogenic segments, marked by a clear change in tectonic regime from contractional to transpressional, is correlated with the southern termination of the craton. The eastern part of the São Francisco craton was strongly remobilized during the formation of the Araçuaí belt. The deformation in the Cabo Frio tectonic domain (CF) is younger than that in the Ribeira/Araçuaí belt and likely represents the westernmost counterpart of the early Cambrian Angola-Congo orogen. The underlying tectonic map is from Cordani et al. (2016). The area delimited by the dotted white lines shows the location of Figure 2. The insert at the lower right corner shows the location of Figure 1 on the northern part of the South America tectonic map of Cordani et al. (2016).

Figure 2: Simplified map of the central Araçuaí belt modified from Vauchez et al., 2007 showing the para-autochthonous cover of the São Francisco cratons and the three main allochthonous units: the western mylonitic unit (WMU), the Central Plutonic Unit (CPU) and the Eastern Anatectic Unit (EAU). Foliation and lineation were either measured in the field or inferred from AMS (Petitgirard et al., 2009; Mondou et al., 2012; Cavalcante et al., 2013). White stars represent cities: GV = Governador Valadares, TO = Teofilo Otoni and BSF = Barra de São Francisco. To/Gd is for Tonalite/Granodiorite and Gr for Granite.

Figure 3: Typical outcrops of the Western Mylonitic Unit (a-c) and of its boundary with the Central Plutonic Unit (d). In the four pictures, west is on the right. a-c show metasediments injected by leucocratic granite and shear criteria that indicate a top-to-the-west sense of shear. In (a), the lenses are leucogranite. (d) shows intercalations of leucogranite, migmatitic metasediments, tonalite (To) free of

solid-state deformation and several asymmetric black lenses resulting from the disruption of an amphibolite layer.

Figure 4: Locations of U/Pb zircon ages (Ma) used in this study. The results (and references) are summarized in Table 1. Symbols: triangles = samples for which only U/Pb zircon ages are available; white hexagon = samples for which both U/Pb zircon ages and $^{40}Ar/^{39}Ar$ age(s) are available (shown in Figure 7). The colors and legends are as in Figure 2.

Figure 5: Pictures of outcrops typical of the Central Plutonic Unit. Tonalites/granodiorites showing a well-developed gently dipping magmatic foliation in the western CPU (a-b) that progressively becomes subvertical eastward (c-d). The subvertical magmatic foliation is underlined by elongated dioritic lenses in (c) and by lenses and discontinuous layers of biotite-rich granite in (d).

Figure 6: Pictures of outcrops typical of the Eastern Anatectic Unit: metatexites (a), diatexites (b) and garnet-rich leucocratic granite (c), all displaying a well-developed foliation that is magmatic in the leucosomes and solid-state in the restitic parts (when present). (d) shows the anatectic kinzigites (kz) at the eastern boundary of the EAU, in which leucogranitic melt focused and formed lenses and veins. The dark lenses in the leucogranite contain garnet + biotite ± cordierite.

Figure 7: Locations of amphibole, biotite and muscovite $^{40}Ar/^{39}Ar$ ages (Ma) used in this study. The numbers in black are the ages obtained in this study, and those in white are previously published $^{40}Ar/^{39}Ar$ ages (4 samples). Diagrams for the newly dated samples are shown in Figures 8 and 9. The analytical data are available in Supplementary Material #3 and #4. Symbols: white hexagons = samples for which both U-Pb and $^{40}Ar/^{39}Ar$ ages are available; black hexagons = samples for which only $^{40}Ar/^{39}Ar$ ages are available. The colors and legends are as in Figure 2.

Figure 8: $^{40}Ar/^{39}Ar$ diagrams for amphibole, muscovite and biotite from samples collected in the Central Plutonic Unit. The diagrams are organized by mineral and for samples from west to east. The analytical data and methodology are available in Supplementary Material #3.

Figure 9: $^{40}Ar/^{39}Ar$ diagrams for biotite from samples collected in the Eastern Anatectic Unit. The diagrams are displayed for samples from north to south. The analytical data and methodology are available in Supplementary Material #4.

Figure 10: Diagram summarizing the data and inferred thermochronological evolutions for the studied domain of the Araçuaí belt. Open squares represent the entire set of U/Pb zircon ages used in this study. Gray squares represent either U/Pb zircon ages of specific samples or the average U/Pb zircon age (Zm) of synkinematic magmatic/anatectic rocks. The temperatures for the zircon data were roughly estimated from (a) the peak temperature (800 °C) and the oldest age (597 Ma) of the Eastern Anatectic Unit, (b) the Zr-in-rutile temperature (780-790 °C) obtained for sample AR-1349 (583 Ma), (c)

equilibrium temperatures (~750 °C) and ages (577-578 Ma) obtained for samples from the Western Mylonitic Unit, and (d) Ti-in-zircon temperatures obtained for several samples from the EAU. For amphibole and biotite, the points in gray with error bars are for individual samples. Am is the average $^{40}Ar/^{39}Ar$ age of amphiboles: Am1 for all dated samples, and Am2 and Am3 are the ages without and for the two oldest samples, respectively. Similarly, Bm is the average $^{40}Ar/^{39}Ar$ age of biotites: Bm1 is for all dated samples, and Bm2 and Bm3 are without and for the two oldest samples, respectively. Line (1) represents the thermochronological evolution based on the average values of all dated samples, (2) excludes the two oldest amphiboles and biotites, (3) is the cooling evolution based on the mean ages of the two oldest amphiboles and biotites, and (4) links the U/Pb zircon age and the $^{40}Ar/^{39}Ar$ biotite age of the oldest sample of the Eastern Anatectic Unit. The error bars for the closure temperature include the dispersion of the estimated grain size and the uncertainties in the diffusion coefficients for amphibole and biotite.

Figure 11: U-Pb zircon ages versus $^{40}Ar/^{39}Ar$ biotite ages in the Eastern Anatectic Unit. The numbers are for the cooling rate calculated for each sample (Table 1). This figure shows the tendency of the age of closure of the K/Ar system in biotite to be correlated with the zircon crystallization ages. Samples showing earlier crystallization of zircon also show earlier closure of the Ar/Ar system in biotite. This suggests a diachronous thermal evolution across the EAU at a nearly constant cooling rate.

Figure 12: Schematic map and cross-section showing the Eastern Anatectic Unit thrust upon the Central and Western Units and, in the northernmost part of the map, directly onto the para-autochthonous metasedimentary cover of the São Francisco craton. The cross-section also shows that the gently dipping basal contact of the EAU crosscuts steeply dipping tectonic contacts and foliation in the eastern part of the CPU, suggesting that the tectonic emplacement of the EAU occurred later than the formation of this subvertical fabric, although it occurred before the anatexites reached solid-state.

Table 1: Summary of U-Pb and $^{40}Ar/^{39}Ar$ ages, grain sizes, closure temperatures and cooling rates obtained from rocks collected in the study area. Zr is for zircon, Am is for amphibole, Ms is for muscovite, and Bt is for biotite. The samples are organized from west to east. (1) indicates ages published in Petitgirard et al. (2009), (2) indicates those published in Mondou et al. (2012), (3) indicates those published in Cavalcante et al. (2018), and (4) indicates those published in Vauchez et al. (2007). The last column shows individual cooling rates calculated for samples for which U-Pb and $^{40}Ar/^{39}Ar$ ages of amphibole and/or biotite have been obtained and for which an initial temperature of the country rock may be inferred. For samples AR-562 (a), AR-590 (b) and AR-1009 (c), ages of 578 Ma, 582 Ma and 583, respectively, were assumed based on their proximity and similarity with dated samples. The cooling rates are indicated as: above the closure temperature of amphibole (>Am), between the amphibole and biotite closure temperatures (Am-Bt) and, for sample AR-648, between the muscovite and biotite closure temperatures (Ms-Bt).

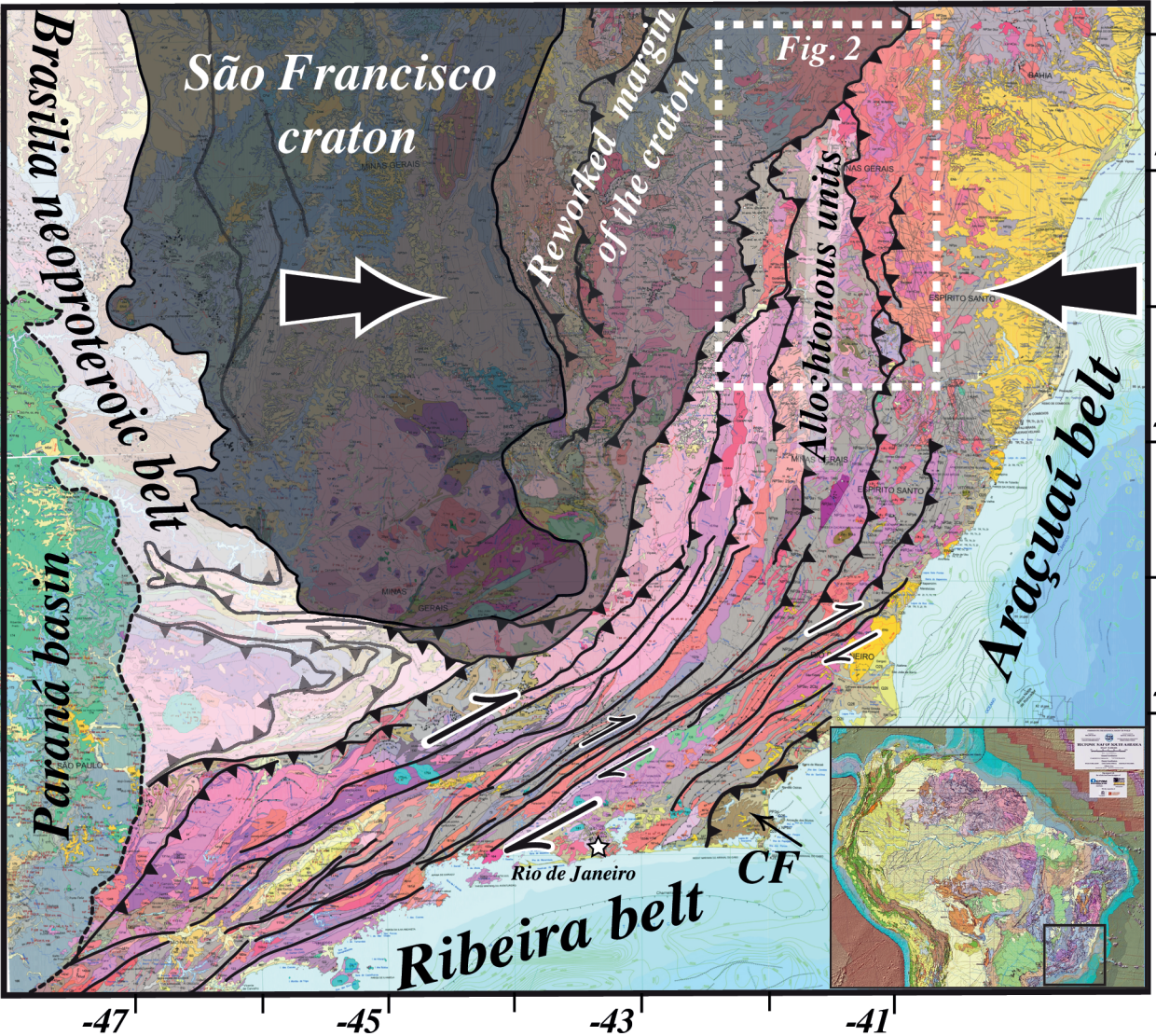

Figure 1: *Schematic map of the Neoproterozoic tectonic belts in eastern Brazil. The Brasilia belt is docked against the western and southwestern boundaries of the São Francisco (SF) craton. The Ribeira/Araçuaí belt formed along the eastern and southeastern boundaries of the craton. The transition between the Araçuaí and Ribeira orogenic segments, marked by a clear change in tectonic regime from contractional to transpressional, is correlated with the southern termination of the craton. The eastern part of the São Francisco craton was strongly remobilized during the formation of the Araçuaí belt. The deformation in the Cabo Frio tectonic domain (CF) is younger than that in the Ribeira/Araçuaí belt and likely represents the westernmost counterpart of the early Cambrian Angola-Congo orogen. The underlying tectonic map is from Cordani et al. (2016). The area delimited by the dotted white lines shows the location of Figure 2. The insert at the lower right corner shows the location of Figure 1 on the northern part of the South America tectonic map of Cordani et al. (2016).*

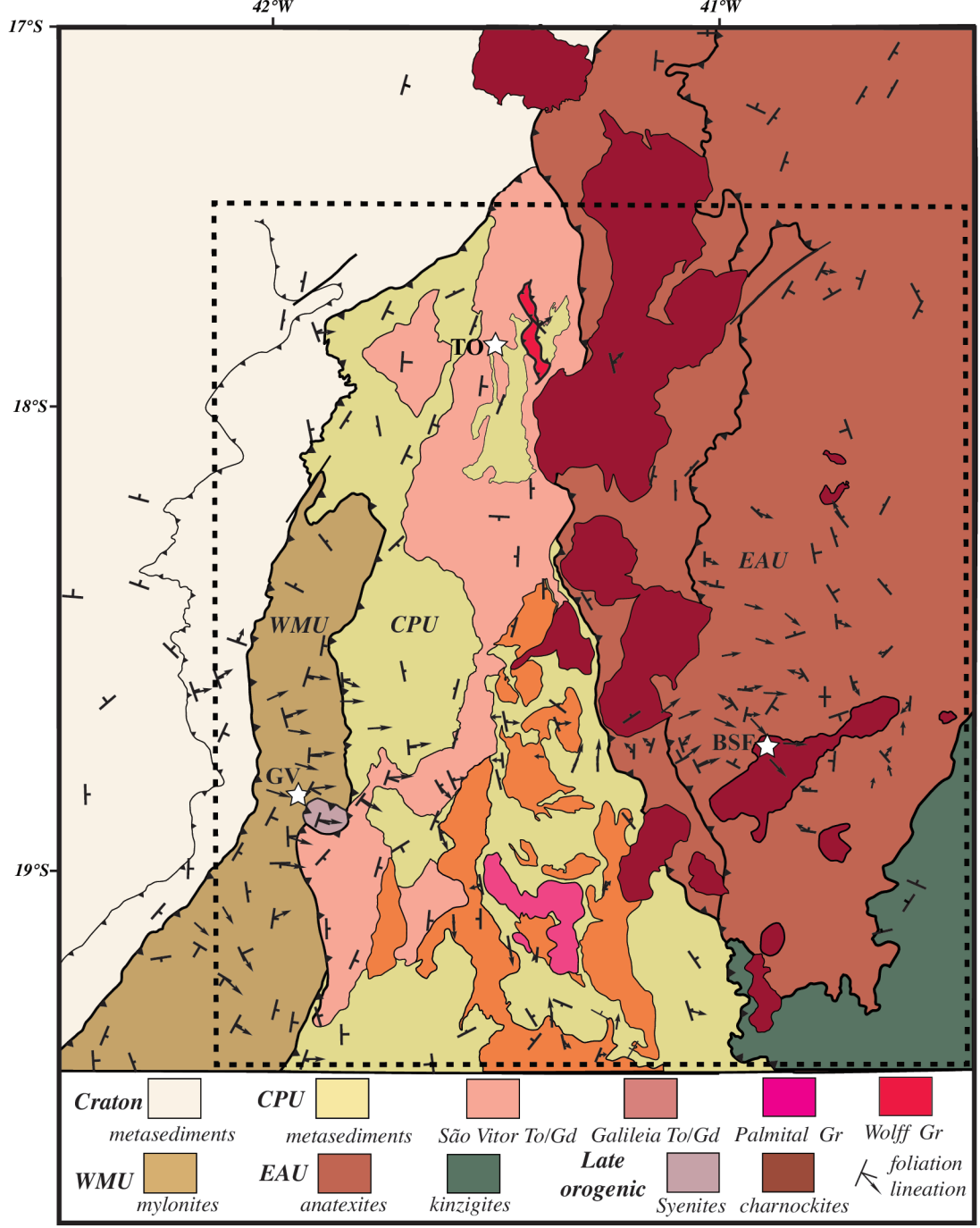

***Figure 2**: Simplified map of the central Araçuaí belt modified from Vauchez et al., 2007 showing the para-autochthonous cover of the São Francisco cratons and the three main allochthonous units: the western mylonitic unit (WMU), the Central Plutonic Unit (CPU) and the Eastern Anatectic Unit (EAU). Foliation and lineation were either measured in the field or inferred from AMS (Petitgirard et al., 2009; Mondou et al., 2012; Cavalcante et al., 2013). White stars represent cities: GV = Governador Valadares, TO = Teofilo Otoni and BSF = Barra de São Francisco. To/Gd is forTonalite/Granodiorite and Gr for Granite.*

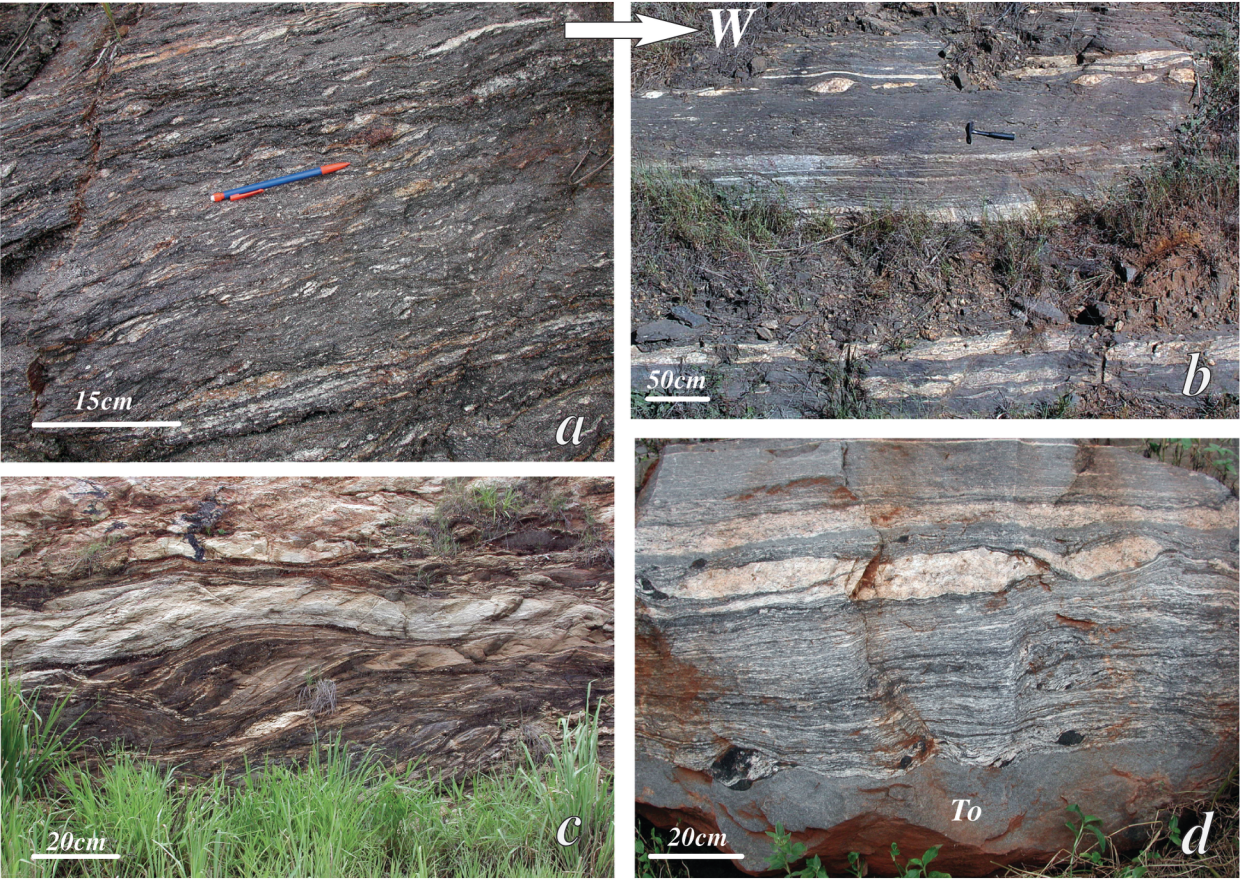

Figure 3: *Typical outcrops of the Western Mylonitic Unit (a-c) and of its boundary with the Central Plutonic Unit (d). In the four pictures, west is on the right. a-c show metasediments injected by leucocratic granite and shear criteria that indicate a top-to-the-west sense of shear. In (a), the lenses are leucogranite. (d) shows intercalations of leucogranite, migmatitic metasediments, tonalite (To) free of solid-state deformation and several asymmetric black lenses resulting from the disruption of an amphibolite layer.*

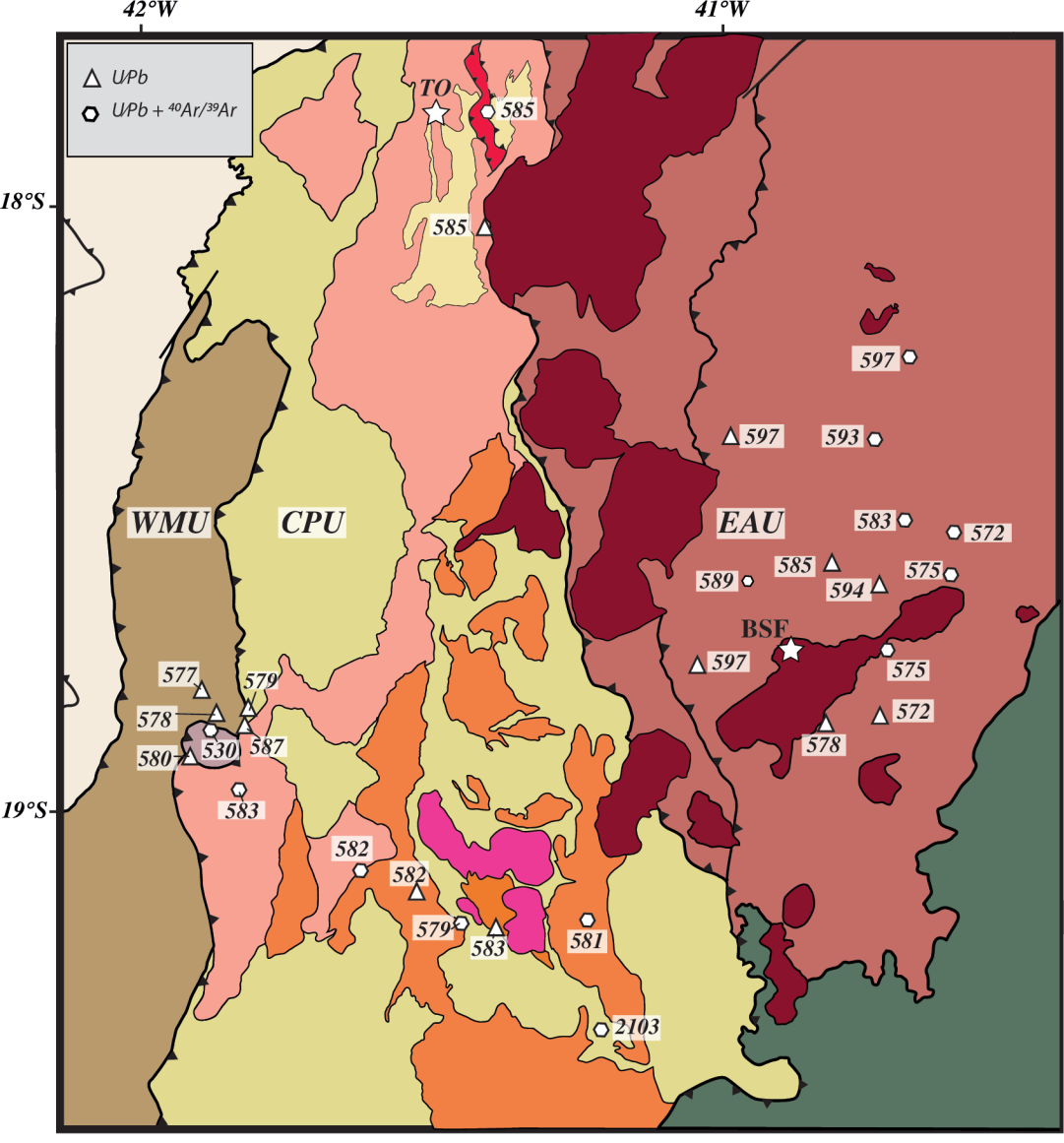

Figure 4: *Locations of U/Pb zircon ages (Ma) used in this study. The results (and references) are summarized in Table 1. Symbols: triangles = samples for which only U/Pb zircon ages are available; white hexagon = samples for which both U/Pb zircon ages and $^{40}Ar/^{39}Ar$ age(s) are available (shown in Figure 7). The colors and legends are as in Figure 2.*

***Figure 5**: Pictures of outcrops typical of the Central Plutonic Unit. Tonalites/granodiorites showing a well-developed gently dipping magmatic foliation in the western CPU (a-b) that progressively becomes subvertical eastward (c-d). The subvertical magmatic foliation is underlined by elongated dioritic lenses in (c) and by lenses and discontinuous layers of biotite-rich granite in (d).*

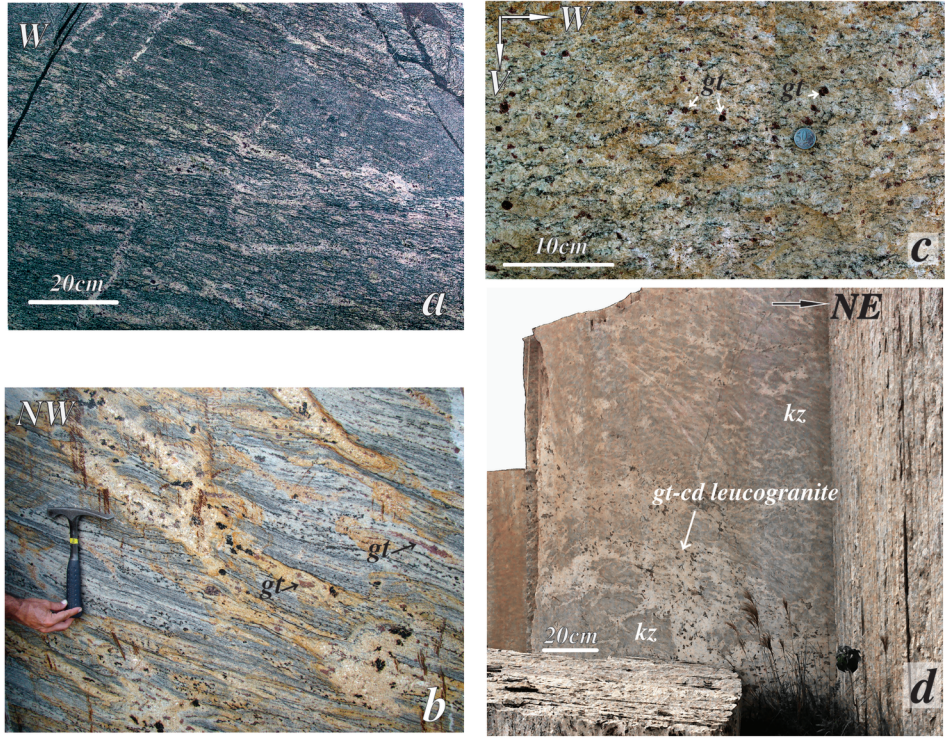

***Figure 6**: Pictures of outcrops typical of the Eastern Anatectic Unit: metatexites (a), diatexites (b) and garnet-rich leucocratic granite (c), all displaying a well-developed foliation that is magmatic in the leucosomes and solid-state in the restitic parts (when present). (d) shows the anatectic kinzigites (kz) at the eastern boundary of the EAU, in which leucogranitic melt focused and formed lenses and veins. The dark lenses in the leucogranite contain garnet + biotite ± cordierite.*

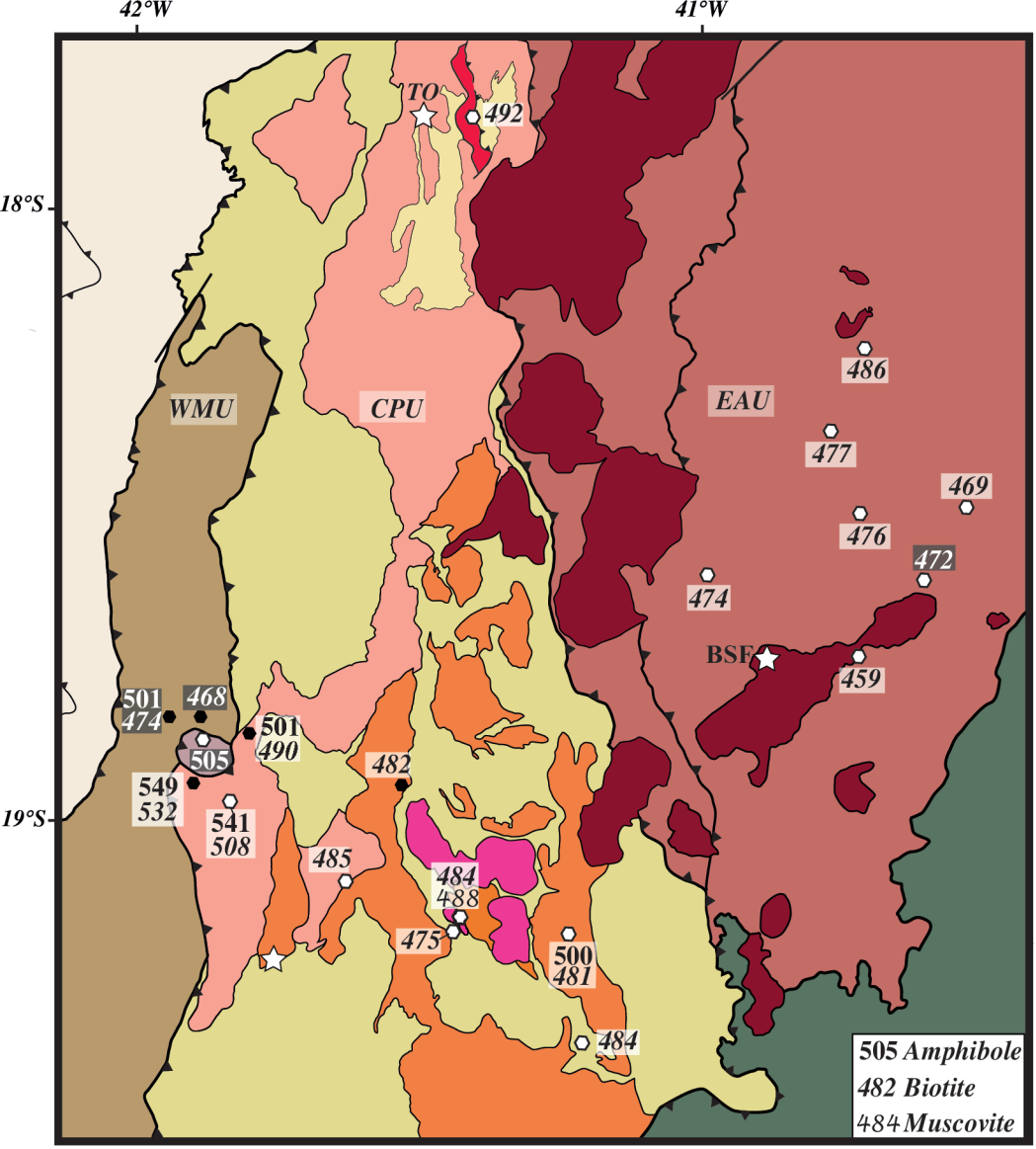

Figure 7 *: Locations of amphibole, biotite and muscovite $^{40}Ar/^{39}Ar$ ages (Ma) used in this study. The numbers in black are the ages obtained in this study, and those in white are previously published $^{40}Ar/^{39}Ar$ ages (4 samples). Diagrams for the newly dated samples are shown in Figures 8 and 9. The analytical data are available in Supplementary Material #3 and #4. Symbols: white hexagons = samples for which both U-Pb and $^{40}Ar/^{39}Ar$ ages are available; black hexagons = samples for which only $^{40}Ar/^{39}Ar$ ages are available. The colors and legends are as in Figure 2.*

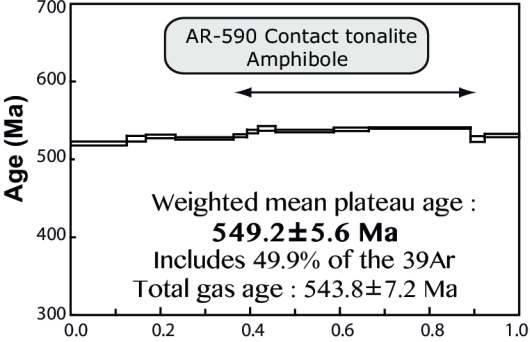
AR-590 Contact tonalite
Amphibole
Age (Ma)
Weighted mean plateau age :
549.2±5.6 Ma
Includes 49.9% of the 39Ar
Total gas age : 543.8±7.2 Ma

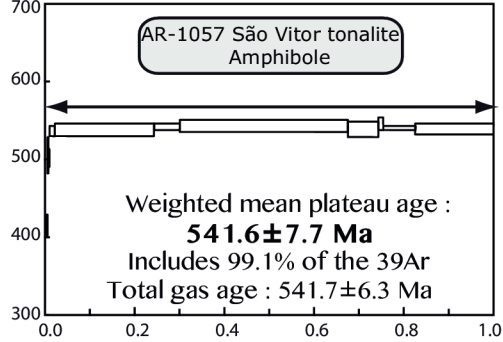
AR-1057 São Vitor tonalite
Amphibole
Weighted mean plateau age :
541.6±7.7 Ma
Includes 99.1% of the 39Ar
Total gas age : 541.7±6.3 Ma

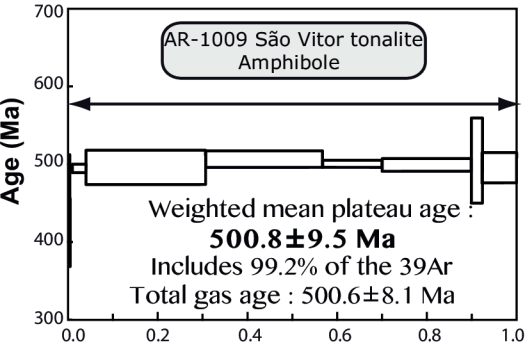
AR-1009 São Vitor tonalite
Amphibole
Age (Ma)
Weighted mean plateau age :
500.8±9.5 Ma
Includes 99.2% of the 39Ar
Total gas age : 500.6±8.1 Ma

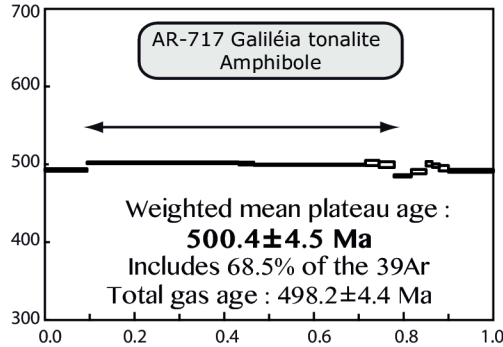
AR-717 Galiléia tonalite
Amphibole
Weighted mean plateau age :
500.4±4.5 Ma
Includes 68.5% of the 39Ar
Total gas age : 498.2±4.4 Ma

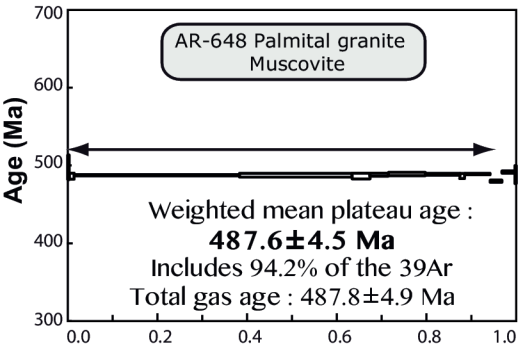
AR-648 Palmital granite
Muscovite
Age (Ma)
Weighted mean plateau age :
487.6±4.5 Ma
Includes 94.2% of the 39Ar
Total gas age : 487.8±4.9 Ma

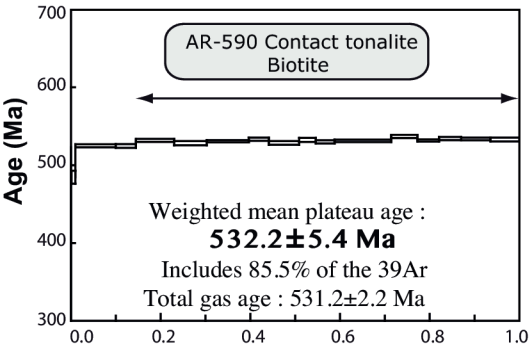
AR-590 Contact tonalite
Biotite
Age (Ma)
Weighted mean plateau age :
532.2±5.4 Ma
Includes 85.5% of the 39Ar
Total gas age : 531.2±2.2 Ma

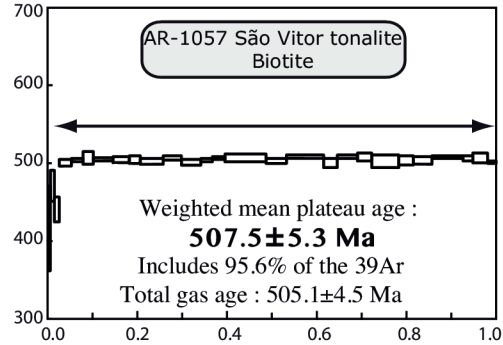
AR-1057 São Vitor tonalite
Biotite
Weighted mean plateau age :
507.5±5.3 Ma
Includes 95.6% of the 39Ar
Total gas age : 505.1±4.5 Ma

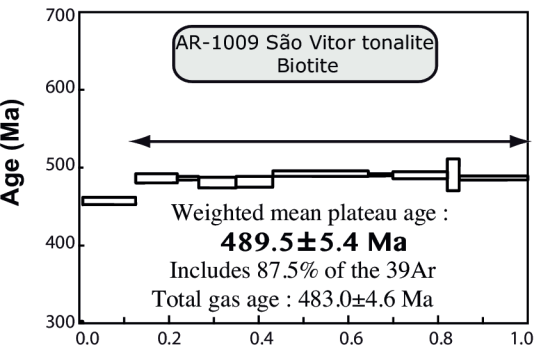
AR-1009 São Vitor tonalite
Biotite
Age (Ma)
Weighted mean plateau age :
489.5±5.4 Ma
Includes 87.5% of the 39Ar
Total gas age : 483.0±4.6 Ma

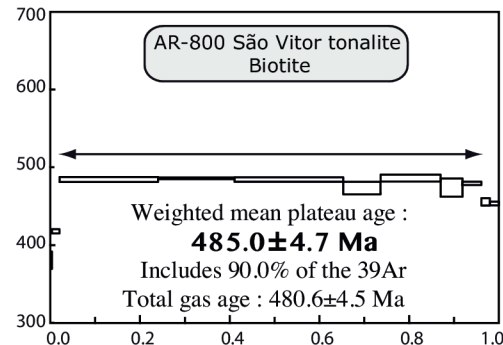
AR-800 São Vitor tonalite
Biotite
Weighted mean plateau age :
485.0±4.7 Ma
Includes 90.0% of the 39Ar
Total gas age : 480.6±4.5 Ma

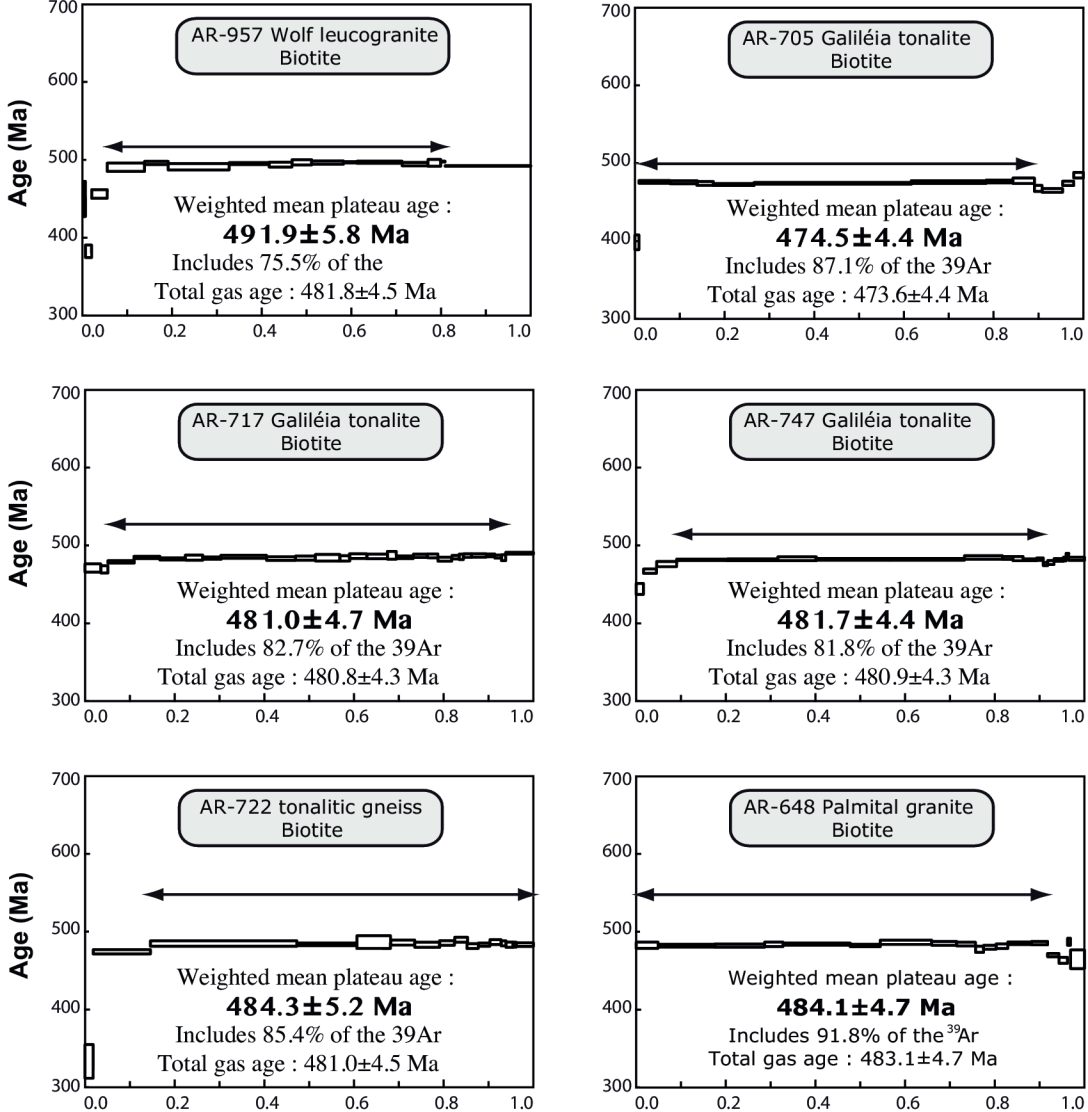

Figure 8: *$^{40}Ar/^{39}Ar$ diagrams for amphibole, muscovite and biotite from samples collected in the Central Plutonic Unit. The diagrams are organized by mineral and for samples from west to east. The analytical data and methodology are available in Supplementary Material #3.*

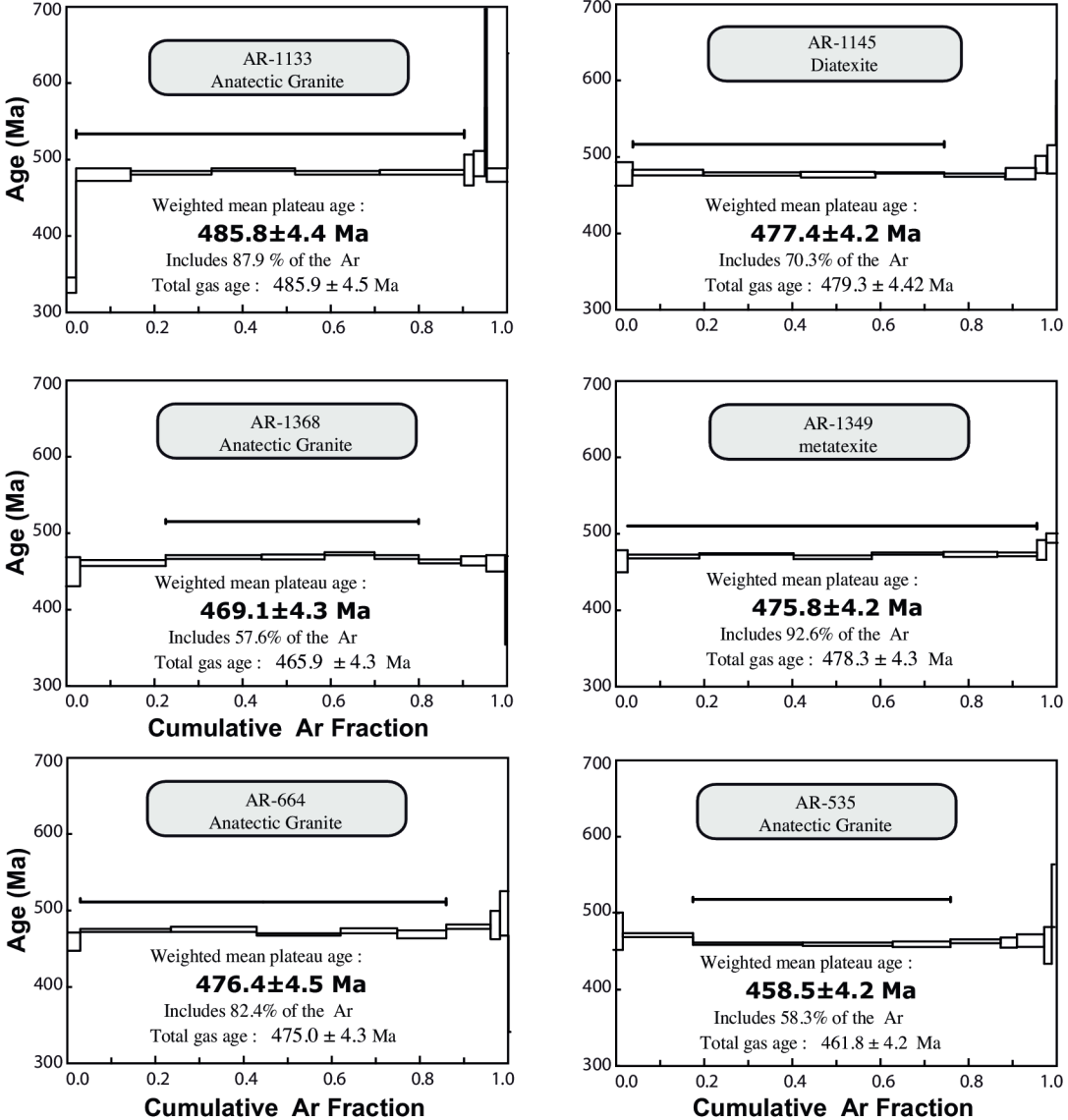

Figure 9: *$^{40}Ar/^{39}Ar$ diagrams for biotite from samples collected in the Eastern Anatectic Unit. The diagrams are displayed for samples from north to south. The analytical data and methodology are available in Supplementary Material #4.*

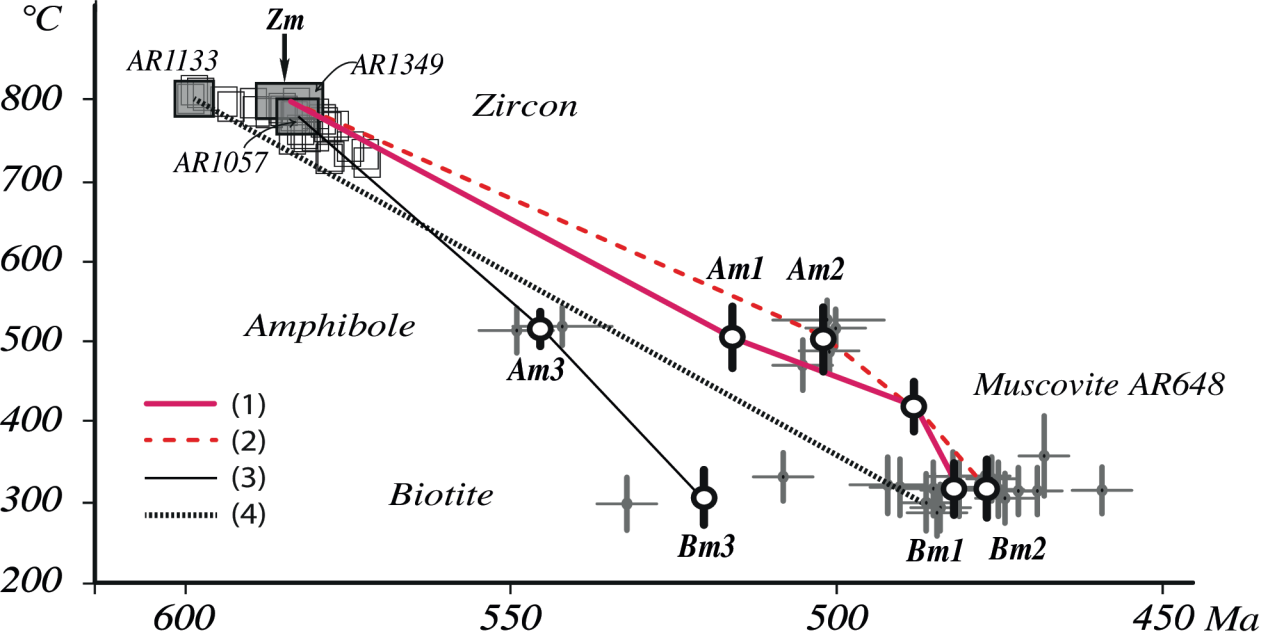

Figure 10: *Diagram summarizing the data and inferred thermochronological evolutions for the studied domain of the Araçuaí belt. Open squares represent the entire set of U/Pb zircon ages used in this study. Gray squares represent either U/Pb zircon ages of specific samples or the average U/Pb zircon age (Zm) of synkinematic magmatic/anatectic rocks. The temperatures for the zircon data were roughly estimated from (a) the peak temperature (800 °C) and the oldest age (597 Ma) of the Eastern Anatectic Unit, (b) the Zr-in-rutile temperature (780-790 °C) obtained for sample AR-1349 (583 Ma), (c) equilibrium temperatures (~750 °C) and ages (577-578 Ma) obtained for samples from the Western Mylonitic Unit, and (d) Ti-in-zircon temperatures obtained for several samples from the EAU. For amphibole and biotite, the points in gray with error bars are for individual samples. Am is the average $^{40}Ar/^{39}Ar$ age of amphiboles: Am1 for all dated samples, and Am2 and Am3 are the ages without and for the two oldest samples, respectively. Similarly, Bm is the average $^{40}Ar/^{39}Ar$ age of biotites: Bm1 is for all dated samples, and Bm2 and Bm3 are without and for the two oldest samples, respectively. Line (1) represents the thermochronological evolution based on the average values of all dated samples, (2) excludes the two oldest amphiboles and biotites, (3) is the cooling evolution based on the mean ages of the two oldest amphiboles and biotites, and (4) links the U/Pb zircon age and the $^{40}Ar/^{39}Ar$ biotite age of the oldest sample of the Eastern Anatectic Unit. The error bars for the closure temperature include the dispersion of the estimated grain size and the uncertainties in the diffusion coefficients for amphibole and biotite.*

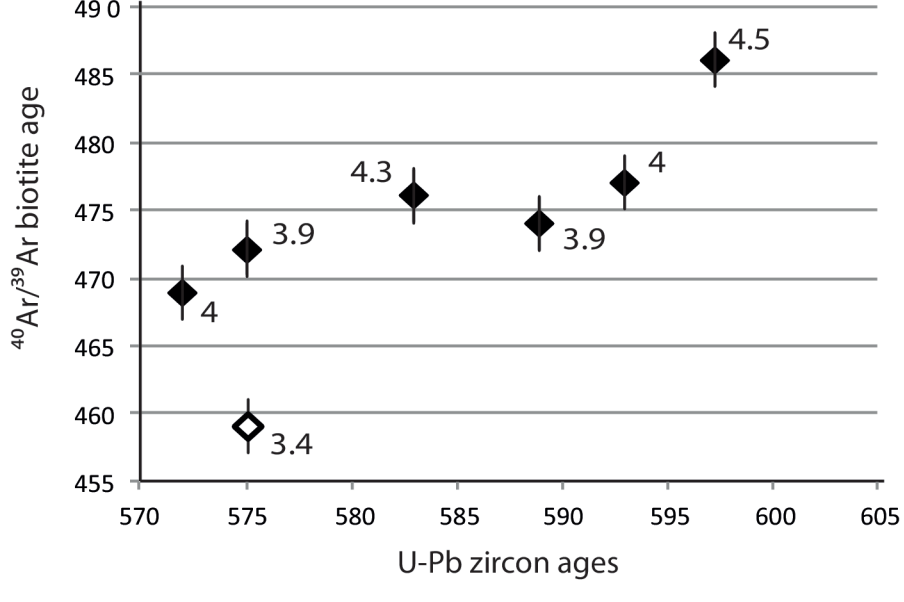

***Figure 11**: U-Pb zircon ages versus 40Ar/39Ar biotite ages in the Eastern Anatectic Unit. The numbers are for the cooling rate calculated for each sample (Table 1). This figure shows the tendency of the age of closure of the K/Ar system in biotite to be correlated with the zircon crystallization ages. Samples showing earlier crystallization of zircon also show earlier closure of the Ar/Ar system in biotite. This suggests a diachronous thermal evolution across the EAU at a nearly constant cooling rate.*

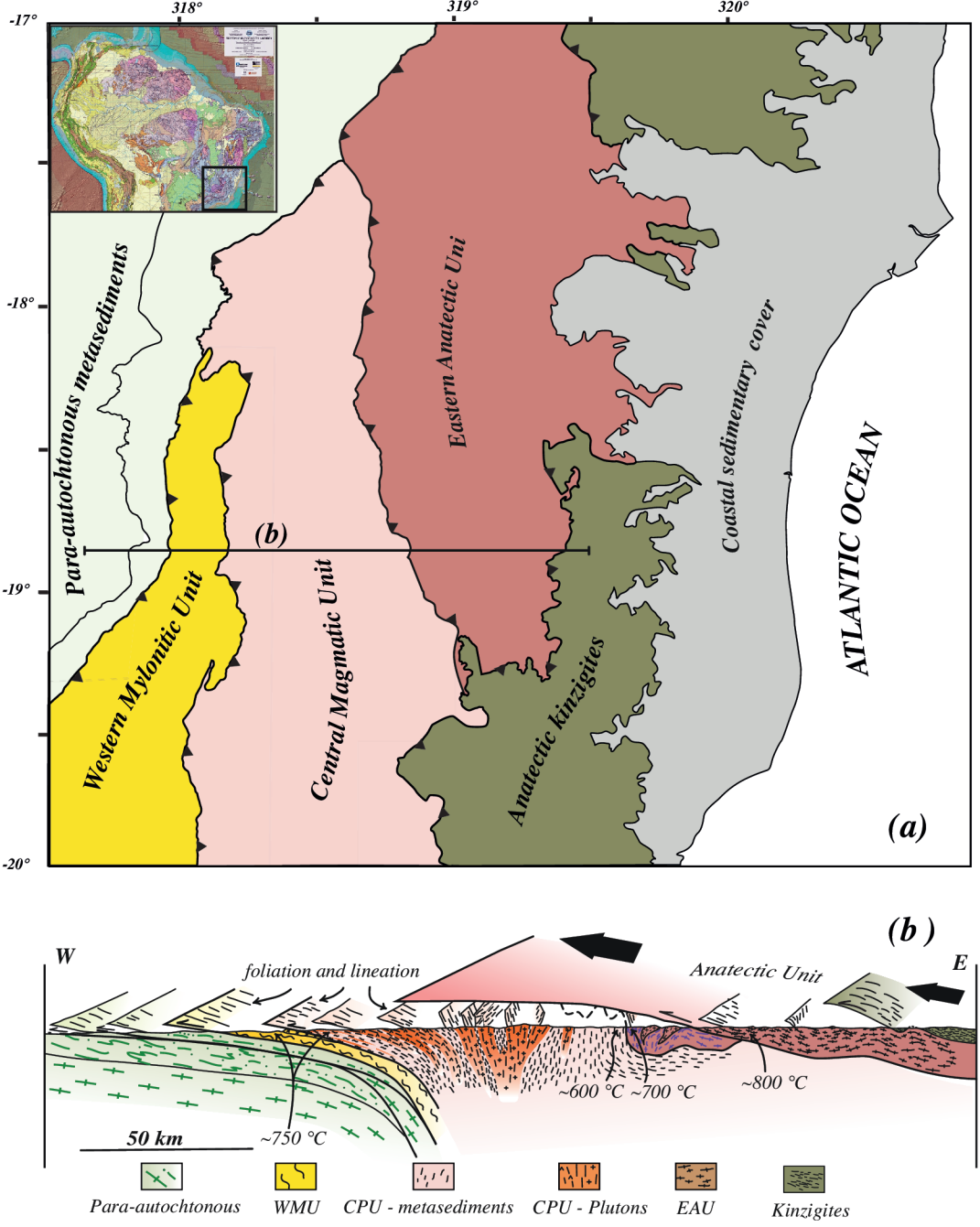

***Figure 12**: Schematic map and cross-section showing the Eastern Anatectic Unit thrust upon the Central and Western Units and even, in the northernmost part of the map, directly onto the para-autochthonous metasedimentary cover of the São Francisco craton. The cross-section also shows that the gently dipping basal contact of the Eastern unit crosscuts steeply dipping tectonic contacts and foliation in the eastern part of the CPU, suggesting that the tectonic emplacement of the EAU is later than the formation of this subvertical fabric, although it occurred before the anatexites reached solid-state.*

	U/Pb Zr *My* (*=^{207}Pb/^{206}Pb)	**^{40}Ar/^{39}Ar** *My*	**Grain size** μm	**Closure T** $°C$	**Cooling rate** $°C/My$
western mylonitic unit	*All data from (1)*		*This work*		
AR-684 leucocratic melt	577±9				
AR-935 leucocratic melt	578±3*				
AR-562 Mylonite		501±5 ((Am) 474±5 (Bt)	200-300 (Am) 100-250 (Bt)	481-495 (Am) 289-313 (Bt)	*3.4[a] (-> Am)* 6.9 (Am-Bt)
AR-86 leucocratic melt		468±4 (Bt)	500-1200 (Bt)	333-360 (Bt)	
AR-414 Ibituruna syenite	530±1	505±5 (Am)	100-200 (Am)	458-481 (Am)	
Contact zone Derribadinha	*Ages from (2)*	This work			
AR-264 Tonalite	581±4				
AR-590 Tonalite		549±6 (Am) 532±5 (Bt)	400-600 (Am) 100-200 (Bt)	505-520 (Am) 289-307 (Bt)	*7.6[b] (-> Am)* 12.6 (Am-Bt)
AR-940 leucocratic melt	587±5				
AR-87 leucocratic melt	579±8				
AR-1057 Tonalite	583±4*	542±8 (Am) 508±5 (Bt)	500-600 (Am) 200-400 (Bt)	513-520 (Am) 307-326 (Bt)	5.7 (-> Am) 5.9 (Am-Bt)
Central plutonic unit	*Ages from (2)*	*This work*			
AR-1009 SV To/Gd		501±9 (Am) 490±5 (Bt)	600-800 (Am) 200-300 (Bt)	520-531 (Am) 307-320 (Bt)	*2.8[c] (-> Am)* 19 (Am-Bt)
AR-800 SV To/Gd	582±6*	485±5 (Bt)	200-400 (Bt)	307-326 (Bt)	4.5 (-> Bt)
AR-968 SV To/Gd	585±7				
AR-957 Wolff leucogranite	585±4	492±6 (Bt)	400-600 (Bt)	326-338 (Bt)	4.5 (-> Bt)
AR-787 Galiléia To/Gd	582±6				
AR-705 Galiléia To/Gd	579±4	475±4 (Bt)	200-400 (Bt)	307-326 (Bt)	4.2 (-> Bt)
AR-815 Galiléia To/Gd	583±4				
AR-717 Galiléia To/Gd	581±4*	500±5 (Am) 481±5 Bt)	500-600 (Am) 200-400 (Bt)	513-520 (Am) 307-326 (Bt)	2.9 (-> Am) 10.5 (Am-Bt)
AR-747 Galiléia To/Gd		482±4 (Bt)	400-600 (Bt)	326-338 (Bt)	
AR-722 orthogneiss	2103±11	484±5 (Bt)	100-150 (Bt)	289-299 (Bt)	
AR-648 Palmital granite		488±5 (Ms) 484±5 (Bt)	200-400 (Ms) 80-120 (Bt)	408-428 (Ms) 283-294 (Bt)	32 (Ms-Bt)
Eastern anatectic unit	*Ages from (3) except AR548*	*All Biotite this work*			
AR-408 Diatexite	597±8				
AR-455 Anatectic granite	594±4				
AR-1133 Anatectic granite	597±3	486±4	150-250	299-313	4.5 (-> Bt)
AR-1145 Diatexite	593±3	477±4	500-600	333-338	4 (-> Bt)
AR-1315 Anatectic granite	597±4				
AR-664 Anatectic granite	589±6	474±4	150-250	299-313	3.9 (-> Bt)
AR- 1349 metatexite	583±5	476±4	400-500	326-333	4.3 (-> Bt)
AR-1358 Anatectic granite	585±4				
AR-535 Anatectic granite	575±3	459±4	400-600	326-338	3.4 (-> Bt)
AR-1119 Diatexite	578±4				
AR-1332 Anatectic granite	572±9				
AR-548 Anatectic granite	575±4 (4)	472±4 (1)	150-300	299-320	3.9 (-> Bt)
AR-1370 Anatectic granite	572±4	469±4	120-300	294-320	4 (-> Bt)

Table 1: Summary of U-Pb and $^{40}Ar/^{39}Ar$ ages, grain sizes, closure temperatures and cooling rates obtained from rocks collected in the study area. Zr is for zircon, Am is for amphibole, Ms is for muscovite, and Bt is for biotite. The samples are organized from west to east. (1) indicates ages published in Petitgirard et al. (2009), (2) indicates those published in Mondou et al. (2012), (3) indicates those published in Cavalcante et al. (2018), and (4) indicates those published in Vauchez et al. (2007). The last column shows individual cooling rates calculated for samples for which U-Pb and $^{40}Ar/^{39}Ar$ ages of amphibole and/or biotite have been obtained and for which an initial temperature of the country rock may be inferred. For samples AR-562 (a), AR-590 (b) and AR-1009 (c), ages of 578 Ma, 582 Ma and 583, respectively, were assumed based on their proximity and similarity with dated samples. The cooling rates are indicated as: above the closure temperature of amphibole (>Am), between the amphibole and biotite closure temperatures (Am-Bt) and, for sample AR-648, between the muscovite and biotite closure temperatures (Ms-Bt).